

Solid-State Properties

Some commercial polymers, particularly polyolefins, are highly crystalline materials with well-defined morphology consisting of chain-folded lamella joined in supramolecular structures called spherulites. Although single crystals of some polymers such as polyethylene can be grown under laboratory conditions, no bulk polymer is completely crystalline. In the case of semicrystalline polymers, regular crystalline units are linked by unoriented, random-conformation chains that constitute amorphous regions. Other polymers may have very low crystallinity characterized by poorly defined crystalline microstructure in an amorphous matrix. An important example of commercial polymer with low crystallinity is poly(vinyl chloride). Many other polymers, such as atactic polystyrene and poly(methyl methacrylate), are totally amorphous. In all cases, morphological aspects such as the presence of crystalline structure have a significant influence on the physical, thermal, and mechanical properties of the polymer. Issues concerning polymer-chain microstructure and the relationship between morphology, bulk properties, and chain conformation

and interchain effects are addressed in this chapter as are methods by which bulk properties can be measured.

4.1 The Amorphous State

Completely amorphous polymers like atactic polystyrene exist as long, randomly coiled, interpenetrating chains that are capable of forming stable, flow-restricting *entanglements* at sufficiently high molecular weight. In the amorphous solid state, chains assume their unperturbed dimensions as they do in solution under θ conditions (see Section 3.1). In the melt, thermal energy is sufficiently high for long segments of each polymer chain to move in random micro-Brownian motions. As the melt is cooled, a temperature is reached at which all long-range segmental motions cease. This characteristic temperature is called the *glass-transition temperature*, or T_g , and varies widely with polymer structure. In the glassy state, at temperatures below T_g , the only molecular motions that can occur are short-range motions of several contiguous chain segments and motions of substituent groups. These processes are called *secondary relaxations*. The concepts of chain entanglements, the glass transition, and secondary-relaxation processes are developed in the following sections.

4.1.1 Chain Entanglements and Reptation

As illustrated by Figure 4-1, polymer chains that are sufficiently long can form stable, flow-restricting entanglements. A good analogy can be made to a bowl of spaghetti. When the individual strands of spaghetti are long, it is very difficult to separate one from the others with a fork; however, when the strands are short, they can be removed easily. Entanglements have significant importance in relation to viscoelastic properties (see Chapter 5), melt viscosity (see Chapter 11), and mechanical properties such as stress relaxation, creep, and craze formation, as will be discussed in this chapter.

Critical Molecular Weight. The minimum polymer chain length or *critical molecular weight*, M_c , for the formation of stable entanglements depends upon the flexibility of a polymer chain and may be directly related to the characteristic ratio, a measure of intramolecular steric hindrance (see Section 3.1) [1]. Relatively flexible polymer chains, such as polystyrene, have a high M_c , while more rigid-chain polymers, such as those with aromatic backbones (e.g., polycarbonate), have a lower M_c . A related parameter is the *molecular weight between entanglements* or M_e . Representative values of M_c and M_e are given in Table 4-1. As a rough rule of thumb, $M_c \approx 2M_e$. Typically, the molecular weight of most commercial polymers

is significantly greater than M_c in order to achieve maximum thermal and mechanical properties. For example, the molecular weight of commercial polystyrene typically falls in the range of 100,000 to 400,000, while M_c is only about 31,200 as given in Table 4-1.

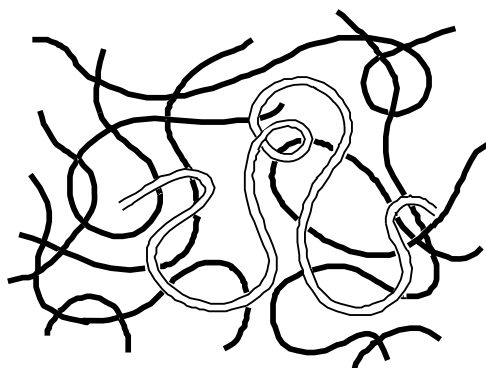


Figure 4-1 Representation of a polymer chain intertwined in a network of entangled chains. Reprinted from Pierre-Gilles de Gennes, *Scaling Concepts in Polymer Physics*. Fig. 11.1, p. 55. Copyright © 1979 by Cornell University. Used by permission of the publisher, Cornell University Press.

Table 4-1 Entanglement Molecular Weights for Linear Polymers^a

Polymer	M_c	M_e
Polycarbonate	4800 ^b	2490 ^c
<i>cis</i> -Polyisoprene	10,000	5800
Polyisobutylene	15,200	8900
Polydimethylsiloxane	24,400	8100
Poly(vinyl acetate)	24,500	12,000
Poly(methyl methacrylate)	27,500	5900
Poly(α -methylstyrene)	28,000	13,500
Polystyrene	31,200	18,100

^a From ref. [2] unless otherwise indicated.

^b From ref. [1].

^c From ref. [3].

Reptation. If individual chains are entangled in the solid state, the question arises as to how long-range movement of chains can occur as the polymer is heated through its T_g and passes from the solid to the melt state. A reasonable explanation has been provided on the basis of the theory of reptation, as originally developed by

Nobel laureate* Pierre-Gilles de Gennes [4] for fixed networks such as a polymer gel and later extended to include melts [5] and concentrated polymer solutions. In the melt state, individual polymer chains can move by local Brownian motion restricted by the topological constraint of neighboring chains. Movement can be visualized as snakelike motion (i.e., reptation) of the chain within a virtual tube, which is defined by the locus of its entanglements with neighboring molecules as illustrated in the top view of Figure 4-2. The theory of reptation has been largely successful in developing a qualitative and quantitative molecular theory for the dynamics and viscoelastic properties of entangled polymers.

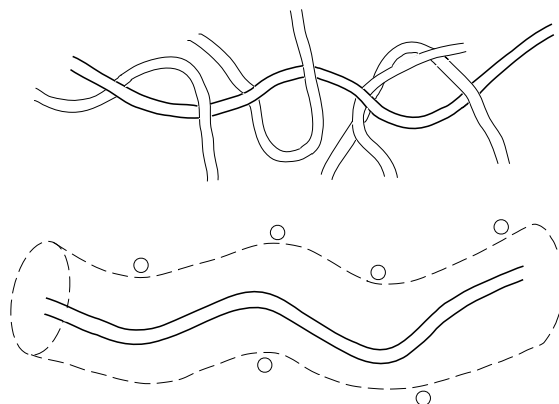


Figure 4-2 Reptation model of a polymer chain constrained in entangled network. A particular chain can be viewed as constrained to move within a virtual tube defined by neighboring entanglement sites. Circles pictured in the lower view represent cross sections of chains constituting the tube constraints. Adapted from J. Klein, *Evidence for Reptation in an Entangled Melt*, Nature, 1978. **271**(5641): p. 143, with permission of the Nature Publishing Group.

4.1.2 The Glass Transition

As mentioned earlier, the temperature that marks the transition from the amorphous solid state to the melt state is called the glass-transition temperature or T_g . Several phenomenological models have been used to provide an understanding of the glass transition. One is that the glass transition marks an *isoviscous* state. This means that, as a polymer is cooled from its melt state, viscosity increases rapidly to a common

* 1991 Nobel Prize in physics.

(maximum) value, ca. 10^{12} Pa-s (10^{13} poise) at T_g , for all glassy materials—both low-molecular-weight and polymeric [6].

A second view is that the glass transition represents a state of *isofree volume*. Free volume, V_f , is defined as the difference between the actual volume (or specific volume), V , of the polymer at a given temperature and its corresponding equilibrium volume at absolute zero, V_o ,

$$V_f = V - V_o . \quad (4.1)$$

The volume at absolute zero can be approximated by the sum of the van der Waals volumes of each chain segment, which can be easily obtained by group-contribution methods [7]. The concept of free volume has significant importance for a number of other related subjects in polymer science, including time-temperature superposition of viscoelastic properties (Chapter 5), melt viscosity (Chapter 11), and permeability (Chapter 12).

A third view of the glass transition is that it represents an *isoentropic* state. This is the foundation of the important Gibbs–DiMarzio theory [8]. Gibbs and DiMarzio have suggested that there is a temperature, T_2 , at which the conformational entropy, S_c (a measure of the total number of ways of arranging a polymer molecule or collection of chains), goes to zero. It can be shown (see Section 5.1.6) that this equilibrium-state temperature lies approximately 52°C below the experimentally measured T_g , which depends upon the *rate* at which the polymer sample is heated or cooled during measurement. As discussed in Chapter 3, polymeric chains can exist in a large number of possible spatial conformations in solution or in the melt state. Each of these conformations corresponds to a different energy state. As the melt is cooled, fewer high-energy conformations are accessible. If the melt is cooled at an infinitely slow rate to ensure the attainment of equilibrium, eventually a temperature will be reached (i.e., T_2) at which only the *lowest-energy* conformation is available. At this point, the conformational entropy will be zero.

The glass-transition temperature of amorphous polymers can vary widely with the chemical structure of the polymer chain. As illustrated by representative values of T_g for several important polymers given in Table 4-2, T_g can vary over a range of 300°C or more. In general, polymers with flexible backbones and small substituent groups (e.g., polyethylene and polydimethylsiloxane) have low T_g , while those with rigid backbones, such as polymers containing main-chain aromatic groups (e.g., polysulfone), have high T_g . A more detailed discussion of structure-property relationships for the thermal transitions of polymers is given in Section 4.3.3.

Table 4-2 Glass-Transition Temperatures of Some Amorphous Polymers

Polymer	T_g (°C)
Polydimethylsiloxane	-123
Poly(vinyl acetate)	28
Polystyrene	100
Poly(methyl methacrylate)	105
Polycarbonate	150
Polysulfone	190
Poly(2,6-dimethyl-1,4-phenylene oxide)	220

4.1.3 Secondary-Relaxation Processes

As previously discussed, secondary-relaxation processes are small-scale molecular motions that can occur in the amorphous glassy state. These can involve limited motions of the main-chain or rotations, vibrations, or flips of substituent groups. An example of a main-chain secondary relaxation that has been proposed is the Schatzki *crankshaft* rotation model illustrated in Figure 4-3. According to this model, five contiguous bonds join in rotation around the main chain consisting of C–C bonds. A simpler crankshaft model proposed by Boyer involves the rotation of three contiguous bonds. Such limited, or non-cooperative, motions may occur at very low temperatures (e.g., ca. -120°C). A discussion of possible molecular motions attributed to the γ -relaxation of polyethylene has been discussed by Boyd and Breitling on the basis of conformational energy calculations [9]. Compilations of major secondary group assignments are given in a variety of sources [10].

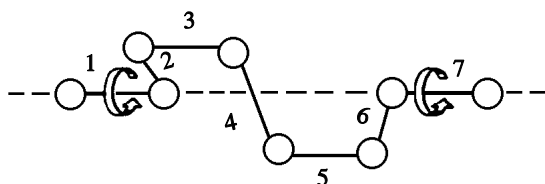


Figure 4-3 Schatzki model of crankshaft motion of a carbon–carbon backbone. The dashed line represents the virtual axis around which bonds 2–6 rotate.

Other examples of main-chain secondary relaxations include rotations of aromatic rings in the backbone of some high-temperature polymers, such as polysulfone and polycarbonate. In addition to these main-chain secondary-relaxation motions, *substituent* groups can rotate or wag at extremely low temperatures in the glassy state. For example, the phenyl ring of polystyrene rotates or wags at 70 K. All these motions can occur in the glassy state, below T_g , as a precursor to the onset

of long-range, main-chain cooperative motions that mark the glass transition. The magnitude and temperature assignment of secondary-relaxation processes can have significant influence on glassy-state properties. For example, the presence of main-chain secondary-relaxation processes has been correlated with impact strength and even with the gas permeability (see Chapter 12) of amorphous polymers.

4.2 The Crystalline State

4.2.1 Ordering of Polymer Chains

Under favorable conditions, some polymers cooled from the melt can organize into regular crystalline structures. Such crystalline polymers have less perfect organization than crystals of low-molecular-weight compounds or low-molecular-weight polymers crystallized from the solution. The basic units of crystalline polymer morphology include crystalline *lamellae* consisting of arrays of folded chains. Reentry of each chain in the folded structure can be adjacent or non-adjacent as illustrated by Figure 4-4. Non-adjacent reentry of chains is illustrated in Figure 4-4A. A chain participating in adjacent reentry can form a tight (or regular) loop (Figure 4-4B) or form a loose (irregular) loop (Figure 4-4C). The thickness of a typical crystallite may be only 100 to 200 Å (10 to 20 nm), indicating that only a portion of the complete chain (e.g., 40 to 80 repeating units in the case of polyethylene) is involved in each fold.

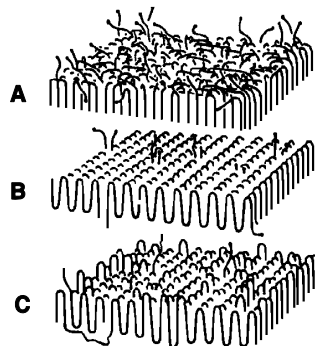


Figure 4-4 Three idealized models for chain folding in polymer crystallites. **A.** Non-adjacent reentry. **B.** Regular adjacent reentry. **C.** Irregular adjacent reentry. Reprinted from J. R. Fried, *Polymer Technology—Part 1: The Polymers of Commercial Plastics*, Plastics Engineering, June 1982. Fig. 7, 38(7), p. 52. Reproduced with permission of Wiley, Inc.

As mentioned earlier, high thermal energy favors a large number of conformations in the melt. As the melt is cooled, the lower-energy conformations are favored, and chains are free to organize into lamellar structure. For many polymers, the lowest-energy conformation is the extended chain or planar zigzag conformation. Such polymers include polyethylene, syndiotactic vinyl polymers, and polymers capable of hydrogen bonding between chains, such as poly(vinyl alcohol) and nylons. In cases of polymers with larger substituent groups, such as the methyl group in polypropylene, for most isotactic polymers, and for polymers of some 1,1-disubstituted ethylenes like polyisobutylene, the lowest-energy conformation is a helix of some preferred geometry [11]. In the case of polypropylene, three repeat units form a single turn in the helix (i.e., 3_1 or 3/1 helix). In the case of polyoxyethylene, there are seven repeat units per two turns (i.e., 7_2 or 7/2 helix). A discussion of the concept of chain conformation and dimension was given in Chapter 3.

For some polymers crystallized from the melt or from concentrated solution, crystallites can organize into larger spherical structures called *spherulites*, as illustrated in Figure 4-5. Each spherulite contains arrays of lamellar crystallites that are typically oriented with the chain axis perpendicular to the radial (growth) direction of the spherulite. In a few cases, such as occurs in the crystallization of polypropylene, chain folding will occur with the chain oriented along the radial direction. The anisotropic morphology of a spherulite results in the appearance of a characteristic extinction cross, or Maltese cross, when viewed under polarized light. During the early stages of crystallization, these supramolecular structures are spherical, but as the level of crystallinity increases, the growing spherulites will eventually meet. Impingement ceases primary crystalline growth and the spherical boundaries are lost.

Since no polymer is completely crystalline, even the most crystalline polymers like high-density polyethylene have lattice defect regions that contain unordered, amorphous material. Semicrystalline polymers may exhibit, therefore, both a T_g corresponding to long-range segmental motions in the amorphous regions and a *crytalline-melting temperature*, or T_m , at which crystallites are destroyed and an amorphous, disordered melt is formed. For many polymers, T_g is approximately one-half to two-thirds of T_m (expressed in Kelvins). Representative values of T_g and T_m for some semicrystalline polymers are given in Table 4-3.

The chemical structure of a polymer determines whether it will be crystalline or amorphous in the solid state. In general, symmetrical chain structures, which allow close packing of polymer molecules into crystalline lamellae and specific interactions between chains that favor molecular orientation, favor crystallinity. For example, linear polyethylene and polytetrafluoroethylene, which have symmetrically substituted repeating units, are highly crystalline. Atactic poly(vinyl chloride) (PVC) with its asymmetrically placed chlorine is highly amorphous. When two chlorine atoms are symmetrically located on the same carbon atom, as they are in poly(vinylidene chloride), crystallinity is again favored.

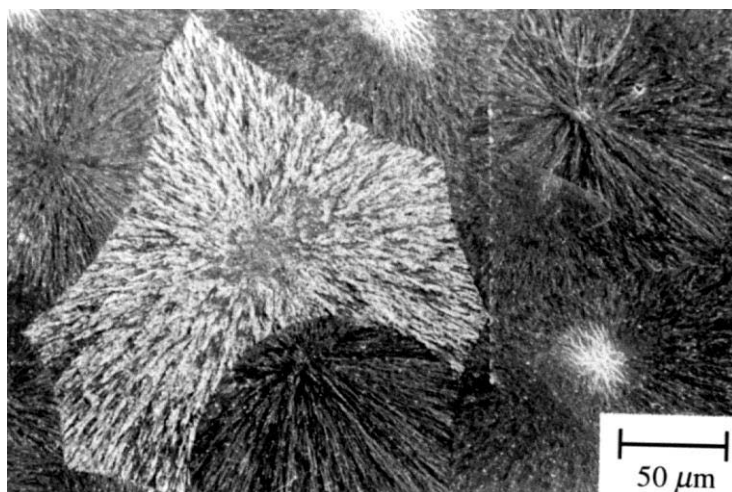


Figure 4-5 Scanning electron micrograph showing the spherulitic structure of polypropylene. The sample was cut using a carborundum-impregnated wire, polished with very fine ($0.1\text{-}\mu\text{m}$) alumina powder, and finally etched using a permanganic acid solution that acts on the amorphous regions of the spherulites to reveal the structure of the lamellae. Polypropylene exists in a number of crystalline forms including a monoclinic α -form (dark areas) and a hexagonal β -form (light areas). The radial structure of the spherulites and impingement of neighboring spherulites are clearly evident in this electron micrograph. Courtesy of M. Aboufaraj, Pechiney Centre de Recherches de Voreppe, France.

Table 4-3 Thermal Transitions of Some Semicrystalline Polymers

Polymer	T_g (°C)	T_m (°C)
Polycaprolactone	-60	61
Polyethylene (high-density)	-120	135
Poly(vinylidene fluoride)	-45	172
Polyoxymethylene	-85	195
Poly(vinyl alcohol)	85	258
Poly(hexamethylene adipamide) (nylon-6,6)	49	265
Poly(ethylene terephthalate)	69	265

Although atactic PVC is amorphous, atactic poly(vinyl alcohol) is partly crystalline because of the occurrence of specific interchain interactions (i.e., hydrogen bonding). Specific interactions are particularly important in enhancing crystallinity in the case of nylons, for which hydrogen bonds can form between an amide carbonyl group on one chain and the hydrogen atom of an amide group on an adjacent chain. Such bonding is illustrated in Figure 4-6 for nylon-6,6, poly(hexamethylene

adipamide). The T_m of nylon-6,6 is 265°C compared to 135°C for polyethylene, which, due to the absence of polar groups, is incapable of participating in interchain interactions.

Both tacticity and geometric isomerism (i.e., a *trans* configuration) favor crystallinity. For example, *cis*-polyisoprene is amorphous, while more easily packed *trans*-polyisoprene is crystalline. Although *cis*-1,4-poly(1,3-butadiene) is partly crystalline, its crystalline form is less stable than the preferred *trans* configuration, as indicated by its lower T_m (2°C) compared to *trans*-1,4-poly(1,3-butadiene) (145°C). In general, tactic polymers with their more stereoregular chain structure are more likely to be crystalline than their atactic counterparts. For example, isotactic polystyrene is crystalline, while commercial-grade atactic polystyrene is amorphous. Commercial-grade suspension-polymerized PVC has a portion of its repeating units in syndiotactic placement and, therefore, has some crystallinity (about 11%). By lowering the temperature of PVC polymerization, syndiotactic placement is favored and the crystalline content will be increased.

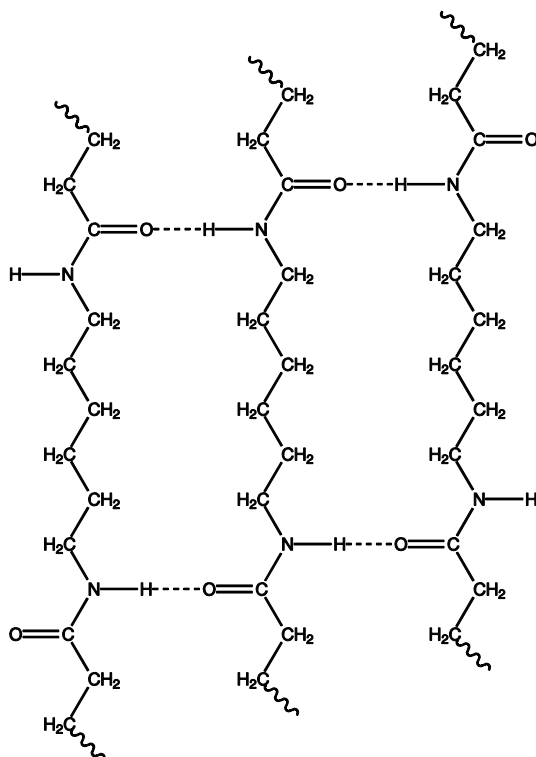


Figure 4-6 Representation of hydrogen bonding between the amide groups in nylon-6,6.

4.2.2 Crystalline-Melting Temperature

From the first law of thermodynamics, the free energy of fusion per repeating unit of the polymer, ΔG_u , can be expressed as

$$\Delta G_u = \Delta H_u - T\Delta S_u \quad (4.2)$$

where ΔH_u and ΔS_u are the enthalpy and entropy of fusion per repeating unit, respectively. At the *equilibrium* melting temperature ($T = T_m^o$), $\Delta G_u = 0$ and, therefore,

$$T_m^o = \frac{\Delta H_u}{\Delta S_u}. \quad (4.3)$$

Some representative values of T_m^o , ΔH_u , and ΔS_u are given in Table 4-4.

Table 4-4 Thermodynamic Parameters for Some Semicrystalline and Crystalline Polymers

Polymer	T_m^o (°C)	ΔH_u (cal mol ⁻¹)	ΔS_u (cal K ⁻¹ mol ⁻¹)
Polyethylene	146	960	2.3
Polyoxymethylene	180	590	3.5
Polypropylene	200	1386	2.9
Poly(ethylene terephthalate)	280	6431	11.6
Polycarbonate ^a	335	6348	10.4

^a Solvent-induced crystallization.

In general, the observed crystalline-melting temperature, T_m , is always lower than the equilibrium value, T_m^o . A number of factors can contribute to this melting-point depression. One is due to the kinetic effect of a finite heating or cooling rate. Another is due to crystallite size, which can be influenced by conditions of the crystallization process or by the presence of impurities. The surface free energy increases with decreasing crystallite size and, therefore, T_m decreases with decreasing size. In addition, the presence of a diluent such as residual solvent or plasticizer can reduce T_m on the basis of thermodynamic considerations. Using the Flory–Huggins theory (see Section 3.2.1), the approximate relation for the melting-point depression of a high-molecular-weight polymer by a diluent is

$$\left[\frac{1}{T_m} - \frac{1}{T_m^o} = \left(\frac{R}{\Delta H_u} \right) \left(\frac{V_u}{V_1} \right) \left(\phi_1 - \chi_{12} \phi_1^2 \right) \right] \quad (4.4)$$

where R is the ideal gas constant, V_u is molar volume per repeating unit of polymer, V_1 is the molar volume of the diluent, ϕ_1 is the volume fraction of the diluent, and

χ_{12} is the Flory interaction parameter between the diluent (component 1) and polymer (component 2). Equation (4.4) indicates that melting-point depression is one way to determine the interaction parameter of a crystallizable polymer in a homogeneous mixture with a solvent, a plasticizer, or a second polymer. Since the presence of a diluent can also decrease T_m by reducing crystallite size, care must be exercised in separating out crystalline size effects from thermodynamic effects [12].

4.2.3 Crystallization Kinetics

For a given polymer, the extent of crystallization attained during melt processing depends upon the rate of crystallization and the time during which melt temperatures are maintained. Above T_m , some polymers that have low rates of crystallization, such as poly(ethylene terephthalate), polycaprolactone, and nylon-6,6, can be quenched rapidly enough to achieve an amorphous state. Other polymers having much higher rates of crystallization, such as polyethylene, cannot be quenched quickly enough to prevent crystallization. For a given polymer, the rate of crystallization depends upon the crystallization temperature, as illustrated by Figure 4-7, which shows the effect of temperature on the rate of spherulite growth in poly(ethylene terephthalate) (PET).

At T_m , the crystalline lamellae are destroyed as fast as they are formed from the melt and, therefore, the net rate of crystallization is zero. Since the large-scale segmental mobility required for chain folding ceases at T_g , the crystallization rate is again zero. At some intermediate temperature, T_{\max} , an optimum balance is reached between chain mobility and lamellae growth. The temperature at which the crystallization rate reaches a maximum is independent of molecular weight; however, the maximum crystallization rate decreases as the molecular weight increases.

The rate of crystallization can be followed by a variety of techniques, such as dilatometric measurement of volume changes, infrared spectroscopy, and optical-microscopic measurement of the growth of spherulite radii with time (e.g., Figure 4-7). During the crystallization process, the fractional crystallinity, ϕ , at time t may be approximated by the *Avrami* equation [13, 14]

$$\boxed{\phi = 1 - \exp(-kt^n)} \quad (4.5)$$

where k is a temperature-dependent growth-rate parameter and n is a temperature-independent nucleation index. Typically, n varies between 1 and 4 depending on the nature of nucleation and growth processes. For example, in the case of sporadically nucleating spherulites, as may result during quiescent melt crystallization near T_m , the nucleation index is approximately 4. The fractional crystallinity of a polymer can be determined by a variety of techniques, including infrared spectroscopy as discussed in Section 2.6.1, density and X-ray diffraction measurements as described

in the next section of this chapter, and by calorimetric methods, which will be described in Section 4.3.2.

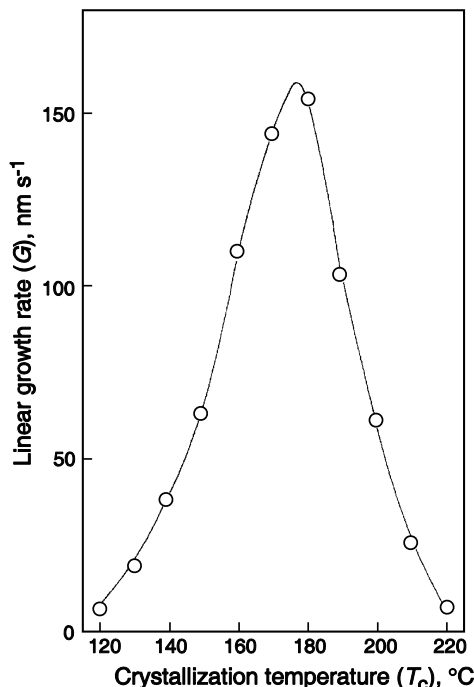


Figure 4-7 Plot of linear growth rate of spherulites in poly(ethylene terephthalate) (PET) as a function of temperature and at a pressure of 1 bar [15]. The maximum growth rate is observed near 178°C. Values of T_g and T_m for PET are approximately 69° and 265°C, respectively.

4.2.4 Techniques to Determine Crystallinity

Density Measurements. Densities can be easily measured at some standard temperature (e.g., 23°C) by means of a calibrated density-gradient column (ASTM* D 792). Once the density (ρ) of the semicrystalline sample has been measured, the fractional crystallinity, ϕ , can be determined as

* See Appendix C for a listing of other important standards.

$$\boxed{\phi = \frac{\rho - \rho_a}{\rho_c - \rho_a}} \quad (4.6)$$

if the densities of a totally amorphous (ρ_a) and totally crystalline sample (ρ_c) are known or can be estimated. Generally, values of amorphous densities are available only for semicrystalline polymers with low crystallization rates that enable rapid quenching from the melt to a totally amorphous state. The crystalline densities of polymers can be obtained from density measurements of single crystals or crystalline low-molecular-weight analogs or may be determined from X-ray determination of crystal densities. Densities for some semicrystalline polymers are given in Table 4-5.

Table 4-5 Amorphous and Crystalline Densities

Polymer	ρ_a (g cm ⁻³)	ρ_c (g cm ⁻³)
Nylon-6	1.09	1.12–1.14
Nylon-6,6	1.09	1.13–1.145
Poly(aryl ether ether ketone) (PEEK)	1.263	1.400
Poly(butylene terephthalate)	1.280	1.396
Poly(ethylene terephthalate)	1.335	1.515
Poly(vinyl chloride)	1.385	1.44–1.53
Polycarbonate	1.196	1.316
Poly(<i>p</i> -phenylene sulfide)	1.32	1.43
Poly(2,6-dimethyl-1,4-phenylene oxide)	1.06	1.31

X-Ray Diffraction. X-ray diffraction is a widely used technique of polymer characterization that can provide information concerning both the crystalline and amorphous states. X-rays are high-energy photons having short wavelengths ($\lambda \approx 0.5$ to 2.5 Å) that interact with electrons. When an X-ray beam is focused on a material, some electrons will be absorbed, some will be transmitted unmodified, while others will be scattered due to interaction with electrons. This interaction results in a scattering pattern that is a function of the scattering angle, usually designated as 2θ for convenience. The scattering pattern provides information on the electron-density distribution and, therefore, the positions of atoms in a polymer. The relationship between the intensity of an (unpolarized) X-ray beam, I_o , the scattered intensity, I , and the scattering angle is given by the *Thomson formula*:

$$I = I_o \frac{K}{r^2} \frac{1 + \cos^2 2\theta}{2}. \quad (4.7)$$

In eq. (4.7), r is the distance between the electron and the detector at which the scattered-beam intensity is measured and K is a constant given as

$$K = \frac{e^4}{m^2 c^4} \quad (4.8)$$

where e ($\approx 1.6022 \times 10^{-19}$ C) and m ($\approx 9.1095 \times 10^{-35}$ kg) are the charge and mass of an electron, respectively, and c is the speed of light ($\approx 3.00 \times 10^8$ m s $^{-1}$).

Terms often used in X-ray scattering are wide-angle X-ray scattering (WAXS) and small-angle X-ray scattering (SAXS). WAXS is used for the investigation of small-scale structures (<10 Å) while SAXS is used to study large-scale morphological features (10 to 10^4 Å). The need to measure the scattered-beam intensity at very small angles (e.g., 0.022° to 2.2°) in relation to the transmitted electron beam in the case of SAXS requires collimators for sharply focusing the incident beam and more specialized detectors than are required for WAXS.

WAXS is used for the determination of fractional crystallinity as well as crystalline dimensions [16]. An example of a WAXS diffraction pattern of a highly crystalline polymer is shown in Figure 4-8. In this case, there is an appearance of several large, narrow peaks positioned upon a broad background pattern. The background pattern is due to scattering from amorphous regions (the amorphous halo), while the peaks, called *Bragg peaks*, represent scattering from well-defined crystalline regions having regular spacing. In many cases, the fractional crystallinity can be estimated by comparing the intensity or height of the amorphous halo (I_{am}) of the crystalline sample with the intensity (I_{am}^0) of a totally amorphous polymer as sometimes can be obtained by rapid quenching from the melt as

$$w_c = 1 - \frac{I_{\text{am}}}{I_{\text{am}}^0} \quad (4.9)$$

where w_c is the *weight* fraction of the crystalline phase.

4.3 Thermal Transitions and Properties

4.3.1 Fundamental Thermodynamic Relationships

Many of the commonly used techniques to determine T_g and T_m can be understood on the basis of the thermodynamic definition of a phase transition originally proposed by Paul Ehrenfest [17] in 1933. A *first-order transition* is defined as one for which a discontinuity occurs in the first derivative of the Gibbs free energy (G). According to the first law of thermodynamics for a reversible, closed system, the

Gibbs free energy can be expressed in differential form as a function of temperature and pressure, $G(T, p)$, as

$$dG = -SdT + Vdp \quad (4.10)$$

where S is entropy and V is the system volume.

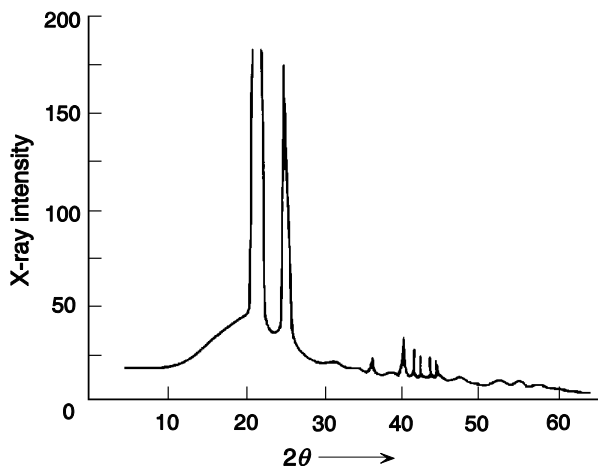


Figure 4-8 X-ray diffraction pattern (WAXS) of high-density polyethylene showing the superposition of crystalline Bragg diffusion peaks on an amorphous background. Adapted from R.-J. Roe, in *The Concise Encyclopedia of Polymer Science and Engineering*, J. I. Kroschwitz, ed. Copyright © 1990 by John Wiley & Sons. This material is used by permission of John Wiley & Sons, Inc.

The free energy may be differentiated with respect to temperature (at constant pressure) as

$$\left(\frac{\partial G}{\partial T} \right)_p = -S \quad (4.11)$$

and with respect to pressure (at constant temperature) as

$$\left(\frac{\partial G}{\partial p} \right)_T = V . \quad (4.12)$$

In terms of describing transitions in polymer systems, the most useful of the preceding relationships is the first derivative with respect to p (eq. (4.12)), which indicates that a *first-order transition should occur as a discontinuity in volume*, as illustrated

in Figure 4-9. Volume is easily measured as a function of temperature by a technique called *dilatometry*, which is described in the next section. The dependence of volume on temperature in the region about the crystalline-melting temperature approximates such a transition (see Figure 4-12).

Second-Order Transitions. The glass transition approximates an Ehrenfest *second-order transition*. This means that a discontinuity should be observed in the *second derivatives* of the Gibbs free energy. Three possible second derivatives can be used to provide a basis for the experimental measurement of T_g . From eqs. (4.11) and (4.12), the corresponding second derivatives are

$$-\left(\frac{\partial^2 G}{\partial T^2}\right)_p = \left(\frac{\partial S}{\partial T}\right)_p, \quad (4.13)$$

$$\left(\frac{\partial^2 G}{\partial p^2}\right)_T = \left(\frac{\partial V}{\partial p}\right)_T, \quad (4.14)$$

and

$$\left[\frac{\partial}{\partial T} \left(\frac{\partial G}{\partial p} \right)_T \right]_p = \left(\frac{\partial V}{\partial T} \right)_p. \quad (4.15)$$

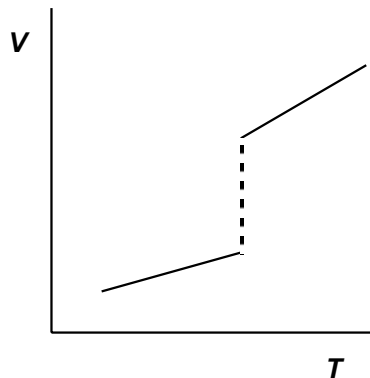


Figure 4-9 Thermodynamic first-order transition in volume at constant pressure.

Since entropy is not an experimentally measurable quantity, eq. (4.13) may be recast into a more useful form in terms of the specific heat at constant pressure, C_p , which is defined as

$$C_p = \left(\frac{\partial H}{\partial T} \right)_P . \quad (4.16)$$

From the first law of thermodynamics, a relation between C_p and entropy can be obtained as^{*}

$$C_p = T \left(\frac{\partial S}{\partial T} \right)_P . \quad (4.17)$$

Substitution of eq. (4.17) into eq. (4.13) indicates that *a second-order transition should occur as a discontinuity in specific heat*, as illustrated in Figure 4-10. Specific heat is easily measured by calorimetric techniques such as differential scanning calorimetry, as described in the next section.

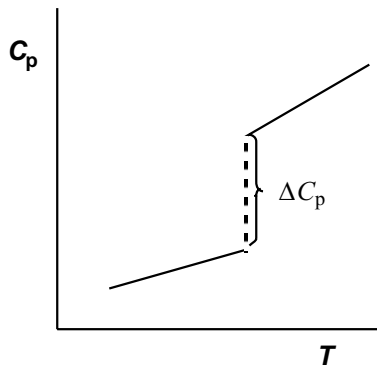


Figure 4-10 Thermodynamic second-order transition in specific heat at constant pressure.

The other two second derivatives indicate that second-order transitions should occur as discontinuities in the slope of volume as a function of pressure (eq. (4.14)) or volume as a function of temperature (eq. (4.15)). These slopes define two useful parameters—the isothermal *compressibility* coefficient, β , and the (isobaric) *thermal-expansion* coefficient, α . As defined earlier, (eqs. (3.73) and (3.74)), these are

* The first law of thermodynamics for a reversible, closed system may be written as

$$dH = TdS + Vdp$$

for which a Legendre transformation gives

$$\left(\frac{\partial H}{\partial T} \right)_P = T \left(\frac{\partial S}{\partial T} \right)_P .$$

$$\beta = -\left(\frac{1}{V}\right) \left(\frac{\partial V}{\partial p}\right)_T \quad (4.18)$$

and

$$\alpha = \left(\frac{1}{V}\right) \left(\frac{\partial V}{\partial T}\right)_p . \quad (4.19)$$

This means that a discontinuity in a plot of α or β versus temperature, or alternatively a change in slope of a plot of volume versus temperature (at constant pressure) or a plot of volume versus pressure (at constant temperature), marks the occurrence of a second-order transition as illustrated in Figures 4-11A and 4-11B, respectively. Both coefficients may be obtained by dilatometric measurements, although the constant-pressure experiment is the easier and, therefore, more commonly used.

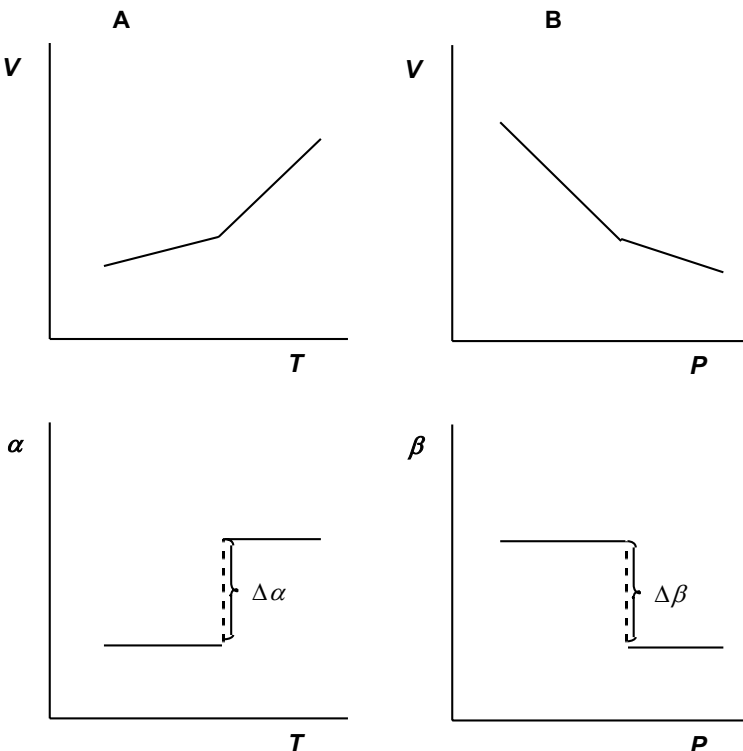


Figure 4-11 **A.** Thermodynamic second-order transition in volume as a function of temperature at constant pressure. **B.** Thermodynamic second-order transition in volume as a function of pressure at constant temperature.

The magnitudes of the discontinuities in C_p , α , and β at the second-order transition may be expressed as

$$\Delta C_p = C_{p,2} - C_{p,1}, \quad (4.20)$$

$$\Delta\alpha = \alpha_2 - \alpha_1, \quad (4.21)$$

and

$$\Delta\beta = \beta_2 - \beta_1 \quad (4.22)$$

where the subscripts, 1 and 2, represent values at temperatures below and above the transition, respectively. These discontinuities are indicated in Figures 4-10 and 4-11.

As illustrated in the next section, the glass transition is not a *true* thermodynamic transition but, rather, it is considered to be a *pseudo*-second-order transition that is influenced by the kinetics of glass formation (i.e., the rate of heating or cooling). Both volume and specific-heat data for polymers closely approximate second-order transition behavior; however, the discontinuities or changes in slope are more gradual and are affected by the heating rate.

4.3.2 Measurement Techniques

A wide variety of experimental methods can be used to determine the glass-transition and crystalline-melting temperatures in polymers. For example, thermal transitions may be detected by changes in refractive index, NMR line width, and birefringence as a function of temperature; however, the most commonly used techniques are dilatometry and, especially, differential scanning calorimetry (DSC), which are described in this section. Another important method of detecting thermal transitions is by recording the response to a cyclical strain (dynamic-mechanical analysis) or electric voltage (dielectric spectroscopy), as will be discussed in Chapter 5. An additional advantage of dynamic-mechanical and dielectric measurements is the ability to detect low-temperature secondary relaxations. By contrast, dilatometric or calorimetric methods are insensitive to the occurrence of secondary-relaxation processes. The glass and melt transitions can also be detected by measurement of modulus as a function of temperature in tensile, stress relaxation, and other mechanical tests, as will be discussed in Section 4.4.2.

Dilatometry. One of the earliest methods used to determine thermal transitions is dilatometry. In this procedure, a small sample of polymer is sealed in a glass bulb to which a precision-bored, calibrated glass capillary is attached. Mercury, whose coefficient of thermal expansion is accurately known, is used to fill the bulb and part of the capillary. The dilatometer is then immersed in a controlled-

temperature bath and the height of the mercury in the capillary is recorded at different temperatures. Heating rate is normally kept very small (1° to 2° min^{-1}) to ensure thermal equilibrium, especially near T_g . From this information, the specific volume of the polymer sample can be obtained as a function of temperature. As illustrated in Figure 4-12, the glass-transition temperature is determined as the temperature at which the volume-temperature curve changes slope (i.e., a discontinuity in α), while at the crystalline-melting temperature (a first-order transition temperature) there is a discontinuity, or step change, in specific volume. Some representative dilatometric data for T_g and thermal-expansion coefficients are given in Table 4-6.

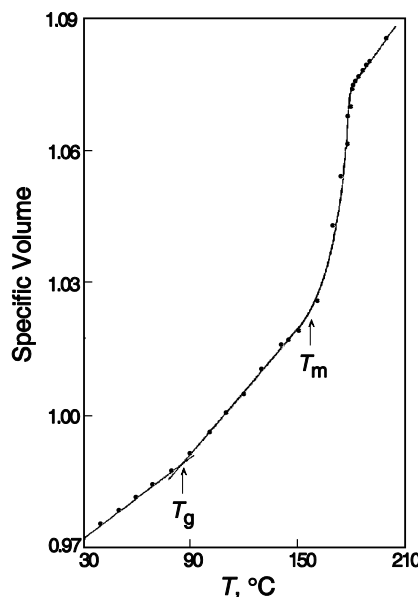


Figure 4-12 Dilatometric data of specific volume of a semicrystalline polymer, poly(*N,N'*-sebacoyl piperazine), plotted against temperature [18]. Results indicate a glass transition near 90°C and a crystalline-melting transition above 160°C .

Table 4-6 Dilatometric Data for Some Representative Polymers [19]

Polymer	T_g (K)	$\alpha' \times 10^4$ (K^{-1})	$\Delta\alpha \times 10^4$ (K^{-1})
Polydimethylsiloxane	150	8.12–12	5.4–9.3
Poly(vinyl acetate)	302	5.98	3.9
Poly(vinyl chloride)	355	5.2	3.1
Polystyrene	373	5.5	3.0
Poly(methyl methacrylate)	378	4.6–5.0	2.45–3.05

As an approximation, the change in thermal-expansion coefficient going from the liquid (i.e., $T > T_g$) to the glassy state (i.e., $T < T_g$),

$$\Delta\alpha = \alpha^l - \alpha^g, \quad (4.23)$$

is sometimes taken to be $4.8 \times 10^{-4} \text{ K}^{-1}$; however, extensive data have shown that $\Delta\alpha$ increases with decreasing temperature, as the data given in Table 4-6 serve to illustrate. As a better approximation, Simha and Boyer [19] have suggested that

$$\Delta\alpha \approx \frac{0.113}{T_g} \quad (4.24)$$

where T_g is in Kelvins.

Calorimetry. One of the most widely used techniques to measure T_g and T_m is differential scanning calorimetry (DSC). This method uses individual heaters to maintain identical temperatures for two small platinum holders—one contains a small (10 to 30 mg) polymer sample mechanically sealed in a small aluminum pan and the other contains an empty (reference) pan, as illustrated in Figure 4-13. Temperatures are measured by use of identical platinum-resistance thermistors. The differential power needed to maintain both the reference and sample pans at equal temperatures during a programmed heating cycle (range of 0.3125° to $320^\circ\text{C min}^{-1}$) is then recorded as a function of temperature.

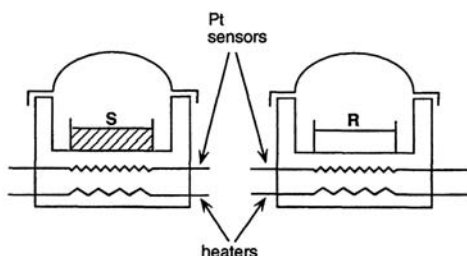


Figure 4-13 Schematic representation of a typical DSC sample cell showing the sample (S) and reference (R) pans, as well as the heating and temperature sensing elements.

In place of differential power, values of specific heat, C_p , may be obtained from the recorded heat-flow rate by calibration with a pure compound such as sapphire for which C_p is known precisely at different temperatures from calorimetry measurements. As illustrated in Figure 4-14, a discontinuity in C_p (i.e., $\Delta C_p = C_p^l - C_p^g$), characteristic of a second-order transition (see the preceding discussion), is observed at the polymer T_g , which is often identified as the temperature at the midpoint of the step change in C_p (i.e., at $\Delta C_p / 2$). For many amorphous

polymers, T_g (K) and ΔC_p ($J\ g^{-1}\ K^{-1}$) are related by the approximate relationship [19] that $\Delta C_p \times T_g \approx 115\ J\ g^{-1}$ ($27.5\ cal\ g^{-1}$).

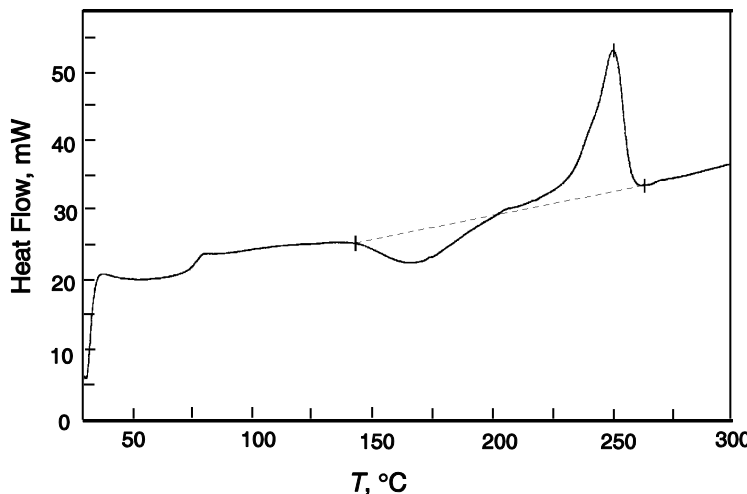


Figure 4-14 DSC thermogram of poly(ethylene terephthalate) crystallized at 200°C for 90 s showing a glass transition near 75°C, an excess crystallization peak above 143°C, and a crystalline-melting endotherm with a peak maximum near 250°C.

During heating of a semicrystalline polymer, additional crystallization may occur at temperatures between T_g and T_m , as illustrated by the crystallization exotherm of poly(ethylene terephthalate) shown in Figure 4-14. At T_m , which may be defined as the extrapolated temperature of the initial slope of the melt endotherm, the crystallites begin to melt over a wide range of temperatures. The breadth of the endotherm is much larger than is typically observed for pure low-molecular-weight compounds as a consequence of the lower order of perfection of polymer crystallites. By calibration with a low-molecular-weight standard such as benzoic acid, the heat of fusion (ΔQ) of a semicrystalline polymer can be determined from measurement of the area under the melt endotherm recorded by DSC. The heat of fusion of the same polymer at 100% crystallinity (ΔH_f) can be estimated from a comparison of the heats of fusion of a homologous series of low-molecular-weight crystals, or from measurement of the melting-point depression of the semicrystalline polymer by diluents (see eq. (4.4)). With this information, the fractional crystallinity (ϕ) of the polymer sample can be obtained by the equation

$$\phi = \frac{\Delta Q}{\Delta H_f}. \quad (4.25)$$

In the case of some polymers, such as isotactic polystyrene with high crystalline order, it is also possible to estimate ϕ from measurement of the specific-heat increment of the semicrystalline polymer at T_g and that of the same polymer in the amorphous state, $(\Delta C_p)_{am}$, obtained by rapid thermal quenching from above T_m , where

$$\phi = 1 - \frac{\Delta C_p}{(\Delta C_p)_{am}}. \quad (4.26)$$

Fractional crystallinity of polymers with low rates of crystallization, such as is the case for polycaprolactone, can be obtained in this manner. For many polymers with low crystalline order, eq. (4.26) will significantly overestimate ϕ because the specific-heat increment of the amorphous phase of the semicrystalline state may be depressed by the presence of small disorganized crystallites that are dispersed in the amorphous matrix.

There have been a number of recent variations of DSC that have broadened its capability of studying thermal events. One is *fast scanning calorimetry* (FSC) that provides scan rates of $750^{\circ}\text{C min}^{-1}$. These high rates allow the study of kinetics of extremely fast processes. Another variation is *temperature-modulated DSC* (TMDSC). The principle behind TMDSC is the superimposition of a periodic modulation of temperature upon a constant heating (or cooling). TMDSC enables the separation of thermal events such as the glass transition from enthalpy relaxation and crystallization as will be described in the following chapter (see Section 5.1.5).

Heat-Distortion Temperature. An alternative, and more applications-oriented, measure of T_g or T_m is called the *heat-distortion* (or heat-deflection) *temperature* (HDT). The HDT is defined by ASTM Standard D 648* as the temperature at which a sample bar of standard dimensions (e.g., $127 \times 13 \times 3$ mm) deflects by 0.25 mm (0.01 in.) under a standard flexural load of 455 kPa (66 psi)[†] placed at its center. The sample is heated in an immersion bath at a rate of $2^{\circ}\text{C min}^{-1}$. In the case of an amorphous polymer, HDT is slightly (10° to 20°C) lower than the T_g as determined by thermal techniques, while in the case of semicrystalline polymers, HDT is more closely identified with T_m , as shown by the values given in Table 4-7. Heat-deflection temperature is, therefore, a useful indicator of the temperature limit above which polymers (or commercial grades of plastics) cannot be used for structural (load-supporting) applications. It is widely used to report the thermal properties of different grades of commercial plastics, including reinforced or filled resins.

* Specification for *tensile* heat-distortion temperature for plastic sheet (0.025 to 1.5 mm in thickness) is given by ASTM D 1637.

[†] A load of 1820 kPa (264 psi) may be specified for a thicker sample.

A listing of other important ASTM standards is given in Appendix C at the end of this text.

Table 4-7 Thermal-Transition Temperatures

Polymer	HDT ^a (°C)	T _g (°C)	T _m (°C)
Polyethylene	29 to 126	-120 to -125	137
Polypropylene	40 to 152	-10 to -18	176
Nylon-6,6	62 to 261	49	265
Poly(vinyl chloride)	60 to 76	87	Low crystallinity
Polycarbonate	39 to 148	150	Amorphous
Polystyrene	63 to 112	100	Amorphous
Polysulfone	146 to 273	190	Amorphous

^a At 1.82 MPa (264 psi); HDT range indicates values reported for all commercial grades that can include filled and other additives.

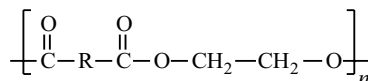
4.3.3 Structure–Property Relationships

As suggested by data given in Tables 4-2 and 4-3, both T_g and T_m are strongly influenced by the chemical structure of the repeating unit. In general, both T_g and T_m increase with decreasing flexibility of the polymer chain. Flexibility decreases with increasing aromatic composition of the main chain or by incorporation of bulky substituent groups or non-rotational groups in the main chain. This is illustrated by the relation of T_m to repeating-unit structure for an analogous series of polyesters in Table 4-8. Replacement of the aliphatic sequence (CH₂)₄ of compound A with an aromatic ring (compound B) increases T_m by 220°C. Replacement by two coupled aromatic rings (compound C) further increases T_m by 85°C, but incorporation of a flexible –CH₂–CH₂– group between aromatic rings lowers T_m by 135°C (compound D). By contrast, incorporation of a non-rotational, unsaturated linkage between aromatic rings (compound E) results in the highest T_m.

Chain flexibility is particularly important in determining T_g. Flexible chains, as may be obtained by incorporating an oxygen atom into the main chain (e.g., polydimethylsiloxane), are capable of large-scale molecular motions at very low temperatures and, therefore, have low T_g. Bulky substituent groups hinder chain rotation and therefore raise T_g as shown by structure–T_g comparisons for several vinyl polymers in Table 4-9. For comparably sized substituent groups, increasing polarity, which may enhance intermolecular interactions, can elevate T_g. This is illustrated by T_g data for the vinyl polymers—atactic polypropylene (T_g = -20°C), poly(vinyl chloride) (T_g = 89°C), and polyacrylonitrile (T_g = 100°C)—given in Table 4-9. As illustrated in Table 4-10, increasing flexibility of the side group can lower T_g, as is evident by comparison of the chemical structures of poly(methyl methacrylate), poly(ethyl methacrylate), and poly(propyl methacrylate). Syndiotac-

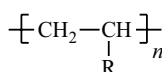
ticity increases T_g as illustrated by data for poly(methyl methacrylate) (PMMA) prepared with different tacticities: *i*-PMMA ($T_g = 45^\circ\text{C}$), *a*-PMMA ($T_g = 105^\circ\text{C}$), and *s*-PMMA ($T_g = 115^\circ\text{C}$). *Trans* geometric isomers have higher T_g than *cis* isomers, as for example in the case of *cis*-polybutadiene ($T_g = -108^\circ\text{C}$) compared to *trans*-polybutadiene ($T_g = -18^\circ\text{C}$) or in the case of *cis*-polyisoprene ($T_g = -73^\circ\text{C}$) compared to *trans*-polyisoprene ($T_g = -53^\circ\text{C}$).

Table 4-8 Effect of Backbone Structure of the Crystalline-Melting Temperature of Polyesters Derived from Ethylene Glycol ($\text{HOCH}_2\text{CH}_2\text{OH}$)



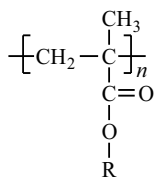
Compound	Main-Chain Unit, R	T_m ($^\circ\text{C}$)
A	—(CH_2) ₄ —	50
B	—(C ₆ H ₄)—	270
C	—(C ₆ H ₄) ₂ —	355
D	—(C ₆ H ₄)—CH ₂ —CH ₂ —(C ₆ H ₄)—	220
E	—(C ₆ H ₄)—CH=CH—(C ₆ H ₄)—	420

Table 4-9 Glass-Transition Temperatures of Selected Vinyl Polymers



Polymer	Substituent Group, R	T_g ($^\circ\text{C}$)
Polyethylene	H	-125
Polypropylene (atactic)	CH ₃	-20
Poly(vinyl chloride)	Cl	89
Polyacrylonitrile	C≡N	100
Polystyrene	(C ₆ H ₅)	100
Poly(α -vinyl naphthalene)	(C ₁₀ H ₇)	135

Table 4-10 Effect of Increasing Size of the Substituent Groups on the Glass-Transition Temperature of Polymethacrylates



Polymethacrylate	Substituent Group, R	T_g (°C)
Poly(methyl methacrylate)	CH ₃	105
Poly(ethyl methacrylate)	CH ₂ CH ₃	65
Poly(propyl methacrylate)	CH ₂ CH ₂ CH ₃	35

4.3.4 Effect of Molecular Weight, Composition, and Pressure on T_g

Molecular-Weight Dependence. The glass-transition temperature increases with molecular weight at low molecular weight but reaches a point at moderate molecular weight where further increase in molecular weight has very little effect on T_g . This is an example of a *limiting-property relationship*. The crystalline-melting temperature, T_m , follows a similar dependence on molecular weight. The particular molecular-weight average most relevant to T_g is the number-average, \bar{M}_n (see Section 1.3.2). This dependence can be rationalized on the basis of the free-volume theory of the glass transition. Since larger free volume is associated with the ends of long polymer chains than with other chain segments, free volume increases with an increasing *number* of chain ends (i.e., decreasing molecular weight).

The form of dependence of T_g on molecular weight is approximated by the Fox–Flory eq. [20]

$$T_g = T_g^\infty - \frac{K}{\bar{M}_n} \quad (4.27)$$

where T_g^∞ is the limiting value of T_g at high molecular weight (obtained from the intercept of a plot of T_g versus reciprocal number-average molecular weight) and K is a constant for a given polymer. Equation (4.27) has been found to give a good fit of experimental data for many polymers; however, there is evidence that K may not be constant for molecular weights below about 10,000 [21]. Representative values of the Fox–Flory parameters, T_g^∞ and K , for some well-characterized polymers are given in Table 4-11.

Table 4-11 Fox–Flory Parameters

Polymer	T_g^∞ (K)	K (K)
Polydimethylsiloxane	148	5.9×10^3
Poly(vinyl chloride)	351	8.1×10^4
Polystyrene	373	1.2×10^5
Poly(methyl methacrylate)	387	2.1×10^5
Poly(α -methylstyrene)	446	3.6×10^5

Composition Dependence. When a second component, either a low-molecular-weight additive or a second polymer, is blended to form a *homogeneous* mixture, the T_g of the mixture will depend upon the amount of each component and upon the T_g of the second component. The form of the T_g –composition dependence may be approximated by several theoretical or semiempirical models.

An approximate relationship between the T_g of a miscible mixture and composition is given by the simple *rule of mixtures*, which for a binary mixture is given as

$$T_g = W_1 T_{g,1} + W_2 T_{g,2} \quad (4.28)$$

where W_i is the weight fraction and $T_{g,i}$ (in Kelvins) is the glass-transition temperature of the i th component (i.e., component 1 or 2 in a binary mixture). For a multi-component mixture, we can write

$$T_g = \sum_{i=1}^N W_i T_{g,i} \quad (4.29)$$

The simple rule of mixtures is a good approximation for blends of two or more polymers but overestimates the T_g of polymers plasticized with a low-molecular-weight organic compound such as an ester or phthalate (see Section 7.1.1).

Improved predictive capability is available through a number of other empirical or theoretical relationships. One of the earliest theoretical expressions is the *Kelley–Bueche equation* [22], which is derived from the isofree volume model of the glass transition. At constant pressure and at a temperature, T , above the glass transition, the fractional free volume, f , is given as

$$f = f_g + \alpha_{f,1} (T - T_{g,1}) \phi_1 + \alpha_{f,2} (T - T_{g,2}) \phi_2 \quad (4.30)$$

where f_g is the fractional free volume at T_g ($f_g \approx 0.025$), α_f is the (isobaric) thermal-expansion coefficient (eq. (4.19)) of the *free volume* of the melt, and ϕ is the volume fraction of the diluent (1) or polymer (2), where $\phi_1 + \phi_2 = 1$. Since the thermal

expansion coefficient of free volume was not a parameter available at the time,* the assumption was made that it was the same as that of the bulk melt state, α , which can be determined by dilatometry (Section 4.3.2) or estimated with good confidence (e.g., eq. (4.24)). By equating T with the T_g of the mixture (whereby $f = f_g$), eq. (4.29) reduces to

$$\alpha_1(T_g - T_{g,1})\phi_1 + \alpha_2(T_g - T_{g,2})\phi_2 = 0 \quad (4.31)$$

which upon rearrangement gives the frequently used Kelley–Bueche expression

$$T_g = \frac{\alpha_1(1 - \phi_2)T_{g,1} + \alpha_2\phi_2T_{g,2}}{\alpha_1(1 - \phi_2) + \alpha_2\phi_2}. \quad (4.32)$$

A more recent relation [23] is based upon a classical thermodynamic treatment of the glass-transition temperature at which the entropies of the glass and liquid phases are equal. The resulting equation for a binary system is given as

$$\ln\left(\frac{T_g}{T_{g,1}}\right) = \frac{W_2\Delta C_{p,2} \ln(T_{g,2}/T_{g,1})}{W_1\Delta C_{p,1} + W_2\Delta C_{p,2}} \quad (4.33)$$

where ΔC_p is the change in specific heat at T_g (see eq. (4.20)). Assuming that the product $T_g\Delta C_p$ is constant for all polymers [24], eq. (4.32) reduces to the simpler form [23]

$$\ln\left(\frac{T_g}{T_{g,1}}\right) = \frac{W_2 \ln(T_{g,2}/T_{g,1})}{W_1(T_{g,2}/T_{g,1}) + W_2}. \quad (4.34)$$

If the T_g s of the polymer and diluent are not too different, a truncated Taylor series expansion of the log terms and rearrangement give the commonly used *inverse rule of mixtures*

$$\frac{1}{T_g} = \frac{W_1}{T_{g,1}} + \frac{W_2}{T_{g,2}}$$

(4.35)

which is known as the *Fox equation* when applied to T_g . The Fox equation has been considered to be an empirical relation; however, the preceding derivation shows that it may be viewed as representing a limiting case of the more general theoretical re-

* It is now possible to determine the thermal expansion coefficient of free volume by use of positron annihilation lifetime spectroscopy.

lationship. Another commonly used empirical relation that can be derived from eq. (4.32) is the *logarithmic rule of mixtures* given as

$$\ln T_g = W_1 \ln T_{g,1} + W_2 \ln T_{g,2}. \quad (4.36)$$

Pressure Dependence. Compared to effects of molecular weight and plasticization, T_g is relatively insensitive to pressure. The glass-transition temperature will increase with increasing pressure at a rate of approximately 25 K per kbar of pressure. The pressure dependence can be estimated from the compressibility and thermal expansion coefficients as

$$\frac{dT_g}{dp} = \frac{\Delta\beta}{\Delta\alpha}. \quad (4.37)$$

Effect of Heating Rate. The T_g has a small dependence on the heating or cooling rates in DSC and other methods of thermal characterization. Samples that are slowly heated through the glass transition exhibit a lower T_g than those that are rapidly heated due to the non-equilibrium state of the glass (see Section 4.1.2). The relationship between T_g (K) and the heating rate, q (K min⁻¹), is given in the form [25, 26]

$$T_g = a + b \ln q \quad (4.38)$$

where a and b are polymer-specific parameters (e.g., $a = 372.5$ K and $b = 4.02$ K for PS; $a = 383$ K and $b = 4.23$ K for PMMA).

Effect of Crosslinks. As a result of the restriction of long-range segmental motion, crosslinking elevates T_g . The form of the relationship between T_g and cross-link density is often given by the Fox–Loshaek equation [27]

$$T_g^c = T_g^o + k_c \rho_c \quad (4.39)$$

where T_g^c is the glass-transition temperature of the crosslinked polymer, T_g^o is the glass-transition temperature of the uncrosslinked polymer, k_c is a polymer-specific constant, and ρ_c represents the number of crosslinks per gram.

4.4 Mechanical Properties

4.4.1 Mechanisms of Deformation

At low strain (i.e., <1%), the deformation of most polymers is elastic, meaning that the deformation is homogeneous and full recovery can occur over a finite time. At higher strains, the deformation of glassy polymers occurs by either *crazing*, characteristic of brittle polymers, or by a process called *shear banding*, which is the dominant mechanism for ductile polymers. Such deformations are not reversible unless the polymer is heated above its glass-transition temperature.

Crazing. The term *crazing* owes its origin to the Middle English word *crasen*, which means “to break.” It was originally applied to describe a network of fine cracks appearing on the surface of ceramics and glasses. When some polymers such as polystyrene are deformed to a certain level, the critical strain (ε_c), what appear to be small cracks develop in a direction *perpendicular* to the principal direction of deformation. Some typical values of critical strains are given in Table 4-12. These crazes reflect light and result in visual cloudiness or whitening of the sample. Crazes developed in a polycarbonate tensile bar are shown in Figure 4-15.

Table 4-12 Critical Strains for Craze Initiation in Glassy Polymers

Polymer	Critical Strain (%)
Polystyrene	0.35
Styrene–acrylonitrile copolymer (SAN)	0.49
Poly(methyl methacrylate)	0.8–1.30
Poly(2,6-dimethyl-1,4-phenylene oxide)	1.5
Polycarbonate	1.8
Polysulfone	2.5

A craze is a unique morphological feature of polymers and is morphologically different from a true crack. A craze, which can be nanometers to a few micrometers in thickness, consists of polymer microfibrils (0.6 to 30 nm in diameter) stretched in the direction of tensile deformation. The microfibrils are surrounded by void space, which can represent as much as 90% of the total volume of the craze. This anisotropic morphology of a craze results in the scattering of light. An electron micrograph of typical craze structures is shown in Figure 4-16.

The time for the initiation of a craze depends upon many factors, including the magnitude of the applied stress, temperature, and the presence of low-molecular-weight liquids, which may act to promote craze development (see Section 6.1.3). Although the reasons for craze initiation are still uncertain and several different theories have been proposed, it is recognized that crazes constitute the defects from

which brittle cracks initiate. Mechanical fracture of a sample that has begun crazing is initiated by the breakdown of the fibrillar microstructure to form additional voids that grow slowly until some critical size has been reached. Beyond this point, the craze will rapidly propagate as a crack. As the crack propagates, crazes are formed at the crack tip and act to retard its advance.

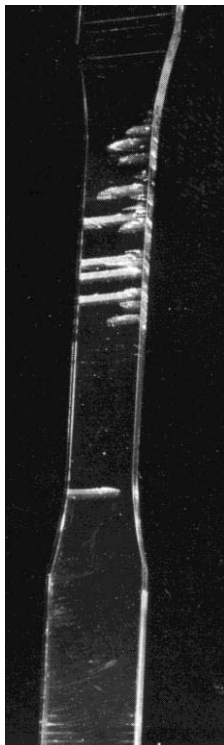


Figure 4-15 Visual view of crazes developed perpendicular to the tensile direction in a polycarbonate dogbone. Courtesy of R. P. Kambour.

Shear Banding. While some polymers such as polystyrene will readily craze when strained in tension, crazes may not develop in other polymers such as polycarbonate under identical conditions. Instead, these polymers will form regions of localized shear deformation. These regions are called shear bands, which develop at angles of 45° to the stretch direction. Other polymers such as SAN can exhibit both modes of deformation. In general, shear-band formation is a dominant mode of deformation during tensile yielding of ductile polymers.

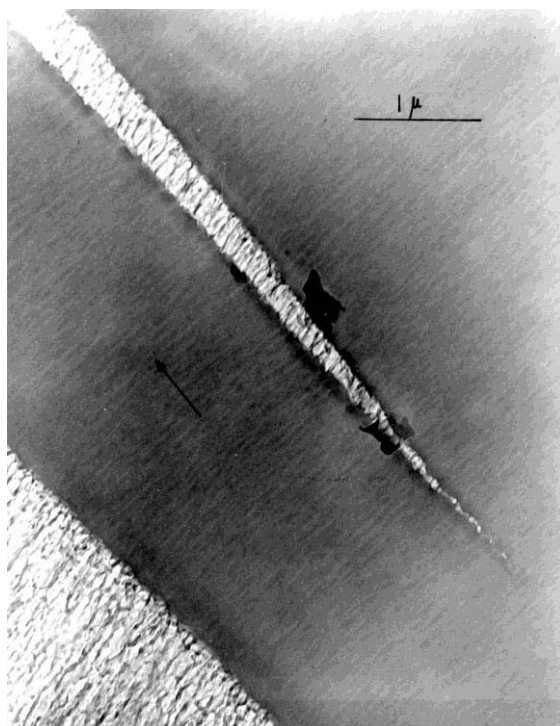


Figure 4-16 Scanning electron micrograph of craze structures in poly(2,6-dimethyl-1,4-phenylene oxide) [28]. The craze structure was preserved prior to microtoming by infusion of liquid sulfur. Courtesy of R. P. Kambour.

4.4.2 Methods of Testing

As the HDT indicates the temperature limits within which a plastic may be used, a variety of methods are used to determine mechanical performance under a variety of loading conditions. These may be classified as static (i.e., tensile and shear), transient (i.e., creep and stress relaxation), impact (Izod and Charpy), and cyclic (i.e., fatigue tests). Static tests are used to measure the force response when a sample is strained, compressed, or sheared at a constant rate. These provide a means to characterize the mechanical properties of a polymer in terms of modulus, strength, and elongation to failure. Transient tests measure the time response of the force (or stress) on a polymer sample when it is rapidly stretched to a given length (*stress relaxation*) or the time response of strain when a load (stress) is rapidly applied (*creep*). Impact tests measure the energy required for a sample to fail under different loading histories, while fatigue tests determine the number of cycles of applied stress required for failure.

Static Testing. Static tests refer to those for which the deformation rate is steady in time. While tensile, compressive, or shear modes may be employed, tensile testing is the most common. In a typical tensile test, a polymer sample, in the form of a dogbone (e.g., Figure 4-17), is clamped at one end and pulled at a constant rate of elongation at the other clamped end.* The thinner portion of the tensile specimen encourages the sample to fail at the center of the bar, where the stress is the highest, and not at the grip sites, where stress concentration may otherwise result in premature failure.

As indicated in Figure 4-17, the initial length of a central section contained within the narrow region of the tensile specimen is called the initial gage length, L_o . During deformation, force, F , is measured as a function of elongation at the fixed end by means of a transducer. Usually, the tensile response is plotted as *engineering* (nominal) stress, σ , versus *engineering* (nominal) strain, ε , where

$$\sigma = \frac{F}{A_o} \quad (4.40)$$

and

$$\varepsilon = \frac{\Delta L}{L_o}. \quad (4.41)$$

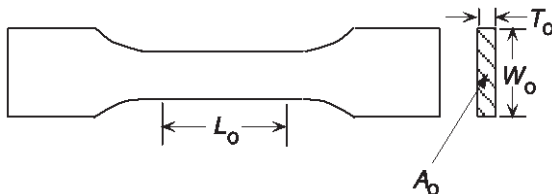


Figure 4-17 Illustration of a typical tensile-dogbone sample. The overall length of the specimens may vary from 63.5 to 246 mm. During tensile measurement, the sample is gripped at the wide ends. Specimen parameters include L_o , gage length (distance between test marks or extensometer span, ca. 50 mm); W_o , initial width (19 or 29 mm); T_o , initial thickness (4 to 14 mm); and A_o , initial cross-sectional area.

In eq. (4.40), A_o is the original (undeformed) cross-sectional area of the gage region and ΔL in eq. (4.41) is the change in sample gage length ($L - L_o$) due to the de-

* Conditions and sample dimensions for tensile tests are specified by ASTM D 638, "Tensile Properties of Plastics." For specimens of thickness up to 3.2 mm (1/8 in.), conditions and sample dimensions are given by ASTM D 1708, "Tensile Properties of Plastics by Use of Microtensile Specimens."

mation. Sample length can be determined from instrumental settings of the mechanical-testing instrument or by an extensometer, which is a strain gage that is attached to the gage-length region of the tensile specimen.

Alternatively, the stress-strain response of a sample may be reported in terms of true stress and true strain. The *true stress* is defined as the ratio of measured force to the *actual* cross-sectional area, A , at a given elongation

$$\sigma^T = \frac{F}{A}. \quad (4.42)$$

Since the actual cross-sectional area decreases as the sample is elongated, the true stress will always be larger than the engineering stress. Assuming that the volume of the sample remains constant during deformation, it can be shown (see Problem 4-1) that the true stress is simply related to the engineering stress as

$$\sigma^T = \sigma \frac{L}{L_0}. \quad (4.43)$$

The *true strain*, ε^T , is defined as

$$\varepsilon^T = \int_{L_0}^L \left(\frac{1}{\ell} \right) d\ell = \ln \left(\frac{L}{L_0} \right). \quad (4.44)$$

With the exception of elastomers, the assumption of a constant volume during deformation is not strictly correct, because the volume of glassy polymers increases, or dilates, during extension. This change in volume, ΔV , at a given strain may be calculated from the relation

$$\Delta V = V - V_0 = (1 - 2\nu) \varepsilon V_0 \quad (4.45)$$

where V_0 is the initial (unstrained) volume, ε is *true* strain, and ν is called *Poisson's ratio*, which is defined as the ratio of *true* strain in the transverse direction, ε_T , to the *true* strain in the longitudinal direction, ε_L , and is calculated as

$$\boxed{\nu = -\frac{\varepsilon_T}{\varepsilon_L} = \frac{1}{2} \left[1 - \frac{1}{V} \left(\frac{\partial V}{\partial \varepsilon} \right) \right].} \quad (4.46)$$

For the majority of glassy polymers, $\nu \approx 0.4$, as shown by data for polystyrene, poly(methyl methacrylate), and poly(vinyl chloride) in Table 4-13. For completely incompressible materials, for which the term $(\partial V/\partial \varepsilon)$ within brackets in eq. (4.46) is zero, ν obtains its maximum value of 0.5 as approached by natural rubber and low-density polyethylene ($\nu = 0.49$).

Hooke's law for an ideal elastic solid provides a relationship between stress and strain for tensile deformation as

$$\boxed{\sigma = E\varepsilon} \quad (4.47)$$

where the proportionality factor, E , is called the tensile (or Young's) modulus. Conversely, the strain and stress are related by the tensile *compliance*, D , defined by

$$\varepsilon = D\sigma. \quad (4.48)$$

For tensile deformation, the compliance is therefore the reciprocal of the modulus

$$D = \frac{1}{E}. \quad (4.49)$$

Table 4-13 Poisson's Ratio of Some Common Polymers

Polymer	Poisson's Ratio
Natural rubber	0.49
Polycarbonate	0.40 ^a
Polyethylene (LD)	0.49
Poly(ethylene terephthalate)	0.43 ^a
Poly(methyl methacrylate)	0.37 ^a
Polystyrene	0.35 ^a
Poly(vinyl chloride)	0.39 ^a

^a From Seitz [29].

As shown by the representative stress-strain plot for a typical brittle polymer in Figure 4-18, only the initial portion of the plot follows Hookean behavior. The point at which stress begins to deviate from a linear stress-strain relation is called the *proportional limit*. This normally occurs before 1% strain. Therefore, to designate a value for the modulus, a convenient procedural definition must be adopted. Consequently, the initial slope of the stress-strain curve is called the *initial modulus*. Alternatively, a line may be drawn from the origin to some convenient point along the stress-strain curve, for example, at 1% strain. This line defines a secant and the slope defines the *secant modulus*, the 1% secant modulus in this case. The modulus, or the compliance, is a *material property* that is a function of both temperature and the time scale of the deformation.

Figure 4-19 shows a representative plot of modulus versus temperature. At temperatures below T_g , all glassy materials, polymeric as well as low-molecular-weight substances, have approximately the same value of modulus (ca. 10^9 Pa or 1 GPa). At first, this modulus slowly decreases with increasing temperature and then rapidly decreases in the region of T_g . For low-molecular-weight materials, modulus continues to fall rapidly with increasing temperature. For high-molecular-weight amorphous polymers, modulus drops to a secondary plateau region (approximately

10^6 Pa or 1 MPa) called the *rubbery plateau*. With further increase in temperature, the modulus again rapidly drops. This point marks the *viscous flow* region. Polymers are typically melt-processed in this temperature range in which the viscosity is also low.

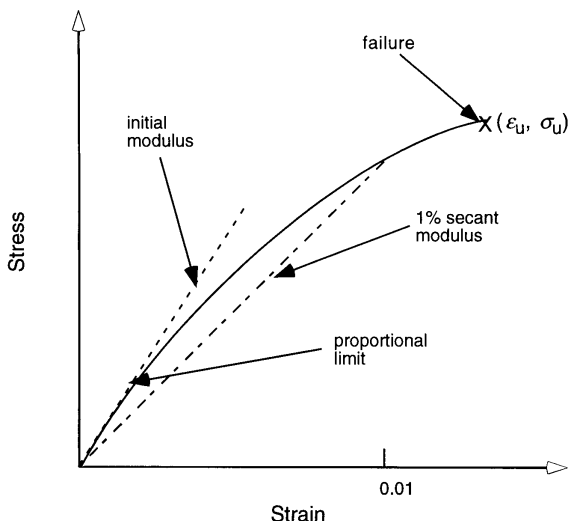


Figure 4-18 Idealized stress-strain curve for a polymer undergoing brittle failure.

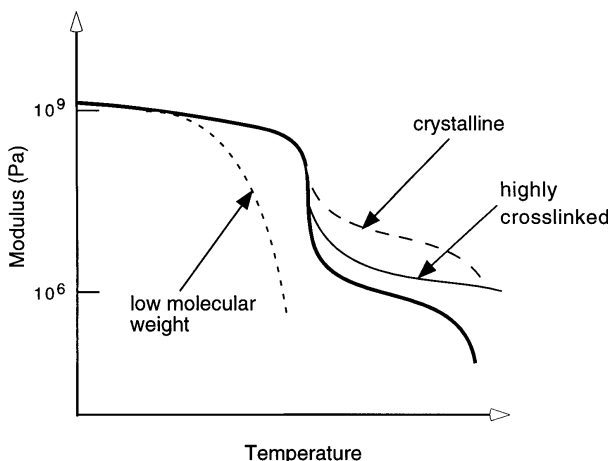


Figure 4-19 Plot of modulus versus temperature for high-molecular-weight amorphous polymers with variations for low-molecular-weight ($M < M_c$), crosslinked, and semicrystalline polymers.

The appearance of a rubbery plateau for high-molecular-weight polymers is the result of the formation of entanglements as described in Section 4.1.1. Entanglements prevent slippage at temperatures immediately above T_g and, therefore, modulus remains relatively high. Above T_g , the entanglements are easily disassociated due to high kinetic energy and the modulus drops. The rubbery plateau modulus, E_p , is inversely proportional to the molecular weight between entanglements, M_e (see Section 4.1.1), as

$$E_p \propto \frac{\rho RT}{M_e} \quad (4.50)$$

where ρ is density.

The temperature behavior of the modulus of semicrystalline polymers is qualitatively similar to that of high-molecular-weight amorphous polymers except that the modulus is typically higher in the secondary plateau (see Figure 4-19) due to the reinforcing effect of crystallites dispersed in an amorphous rubbery phase at temperatures above T_g but below T_m . At T_m , the crystallites melt and the modulus drops in the viscous-flow region.

In addition to tensile deformation, samples may be *compressed* (ASTM D 695) or *sheared*. In the case of compression, the sample is typically prepared in the form of a disk. The measured parameters are the bulk modulus, K , and compliance, B . A simple shear deformation of a solid is illustrated in Figure 4-20. The engineering *shear stress*, τ , is defined as

$$\tau = \frac{F}{A_o} \quad (4.51)$$

where A_o is the area of the *surface* on which the shear force acts. The shear strain, γ , is given by the angle of deformation, θ , as

$$\gamma = \tan \theta = \frac{\Delta X}{C}. \quad (4.52)$$

Hooke's law for shear deformation is given as

$$\tau = G\gamma \quad (4.53)$$

where G is the shear modulus, while the shear compliance is normally designated as J ($\equiv 1/G$).

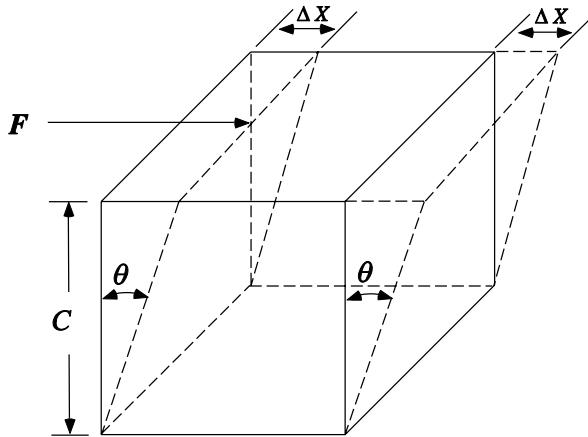


Figure 4-20 Illustration of the shear deformation of a solid with the shear force (F) acting on the top surface of the cube.

Moduli obtained in different deformation modes (tensile, compression, and shear) may be interrelated through Poisson's ratio, ν . For *isotropic* materials, the following relationships hold:

$$E = 2(1 + \nu)G, \quad (4.54)$$

$$J = 2(1 + \nu)D, \quad (4.55)$$

and

$$K = \frac{E}{3(1 - 2\nu)}. \quad (4.56)$$

In the limit of incompressibility (i.e., $\nu = 0.5$), eqs. (4.54), (4.55), and (4.56) reduce to

$$E = 3G, \quad (4.57)$$

$$J = 3D, \quad (4.58)$$

and

$$K \rightarrow \infty, \quad (4.59)$$

respectively. The limiting behavior for bulk modulus expressed by eq. (4.59) simply means that *incompressible* materials cannot be compressed.

Polymers exhibit a wide range of mechanical behavior depending upon temperature and rate of deformation. Typical stress-strain curves covering this range of

behavior are illustrated in Figure 4-21. At normal use temperatures, brittle polymers (e.g., polystyrene) exhibit a rapid increase in stress with increasing strain (i.e., high modulus) up to the point of sample failure (curve 1). The stress at failure is called the *ultimate stress* (σ_u) or stress-at-break (σ_b). Unlike modulus, ultimate stress, resulting from large and irreversible deformation, is a *sample* rather than material property and is strongly influenced by sample defects and processing history. For this reason, a sufficiently large number of samples must be evaluated and their values averaged in order to get a statistically meaningful value.

Ductile polymers, including many engineering thermoplastics, polyamides, and toughened (rubber-modified) plastics, exhibit stress-strain behavior represented by curves 2 and 3 in Figure 4-21. As shown, the stress reaches a maximum value, which is called its *yield stress*, σ_y , at a certain strain, ε_y . As strain is further increased, stress at first decreases. This process is called *strain softening*, which usually occurs at strains between 5% and 50%. A minimum in stress reached during strain softening is called the *draw stress*. At this point, the sample may either fail (curve 2) or experience *orientation hardening* (curve 3) prior to failure. During orientation hardening, polymer chains are stretched locally in the tensile direction. Chain extension causes a resistance to further deformation; stress is, therefore, observed to increase. Accompanying the molecular processes that are occurring during orientation are macroscopic changes in the shape of the tensile specimen. Above the yield point, a portion of the tensile dogbone begins to locally decrease in width or *neck* within the gage region. If orientation hardening occurs before sample failure, the neck is said to stabilize. This means that no further reduction in a cross-sectional area occurs and the neck propagates along the length of the gage region until the sample finally breaks. This process of neck propagation is called *cold drawing*.

The initial slope of the stress-strain plot for ductile polymers (curves 2 and 3 in Figure 4-21) is smaller than that observed for polymers that fail in a brittle mode (curve 1). In other words, the modulus of ductile polymers is lower. On the other hand, the energy required to deform the sample to the point of failure is much higher for ductile polymers, as indicated by comparison of the areas under the stress-strain curves for a brittle (curve 1) and for a ductile polymer (curve 3). This means that ductile polymers are able to absorb more energy upon impact.

Rubber polymers follow stress-strain behavior similar to that of curve 4. Modulus is low, but ultimate extension can be very high, on the order of several hundred percent. Before failure, the rubber may experience an increase in stress as a consequence of strain-induced crystallization caused by molecular orientation in the stretch direction, as discussed in Chapter 5.

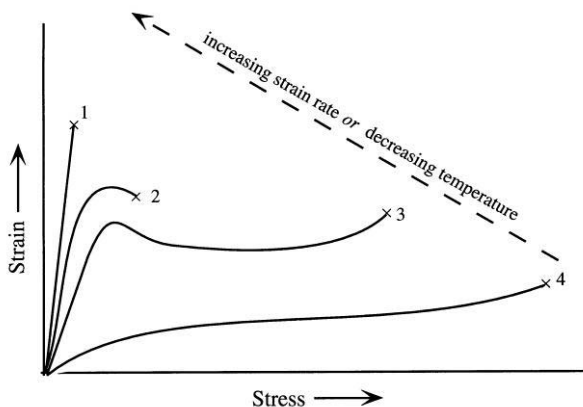


Figure 4-21 Typical stress-strain curves for samples exhibiting brittle failure (curve 1), ductile failure with neck formation (curve 2), ductile failure with cold drawing and orientational hardening (curve 3), and rubbery behavior with evidence of strain-induced crystallization (curve 4). Point of failure is indicated by the symbol \times .

Typical values of modulus, yield strength (stress-at-yield), ultimate strength (stress-at-break), and elongation-to-break for a variety of important thermoplastics are given in Table 4-14. The exact nature of the tensile response of a polymeric material depends upon the chemical structure of the polymer, conditions of sample preparation, molecular weight, molecular-weight distribution, crystallinity, and the extent of any crosslinking or branching. The mechanical response also depends in a very significant way on temperature and the rate of deformation. As illustrated by Figure 4-21, any amorphous polymer can exhibit the entire range of tensile behavior, from brittle to rubbery response, by increasing the testing temperature from room temperature to above the T_g of the polymer or (to a lesser extent) by decreasing the rate of deformation.*

The combined effect of temperature and strain rate on the stress-strain curve of an elastomer can be represented by a *failure envelope*, as shown in Figure 4-22. The ordinate is nominal stress-to-break normalized to an arbitrary reference temperature. All values of ultimate strength obtained over a wide range of temperatures and strain rates comprise points on the outer failure envelope (heavy curve). The curves originating at the origin are selected stress-strain curves at different temperatures and strain rates. As the failure envelope shows, either increasing the strain rate or

* It should be noted that polymers that appear brittle in tensile tests can appear to yield when tested in compression at the same temperature.

decreasing the testing temperature causes the ultimate strength of the sample to decrease.

Table 4-14 Mechanical Properties of Representative Polymers

Polymer	Elastic Modulus (GPa) ^a	Yield Strength (MPa)	Ultimate Strength (MPa)	Elongation to Break (%)
Polycarbonate	2.4	55–69	55–69	60–120
Polyethylene (low-density)	0.14–0.28	6.9–14	10–17	400–700
Poly(methyl methacrylate)	2.4–2.8	48–62	48–69	2–10
Polypropylene	1.0–1.6	23	24–38	200–600
Polystyrene	2.8–3.5	—	38–55	1–2.5
Polytetrafluoroethylene	0.41	10–14	14–28	100–350
Poly(vinyl chloride) (rigid)	2.1–4.1	55–69	41–76	5–60

^a To convert GPa to psi, multiply by 1.45×10^5 ; to convert MPa to psi, multiply by 145.

Transient Testing. As mentioned earlier, two types of transient mechanical tests are creep and stress-relaxation measurements, which can be used to characterize the dimensional stability of a material. A creep test measures the elongation of a specimen subjected to a rapid application of a constant load, σ_0 , at constant temperature. By contrast, a stress-relaxation test records the stress required to hold a specimen at a fixed elongation, ε_0 , at constant temperature.

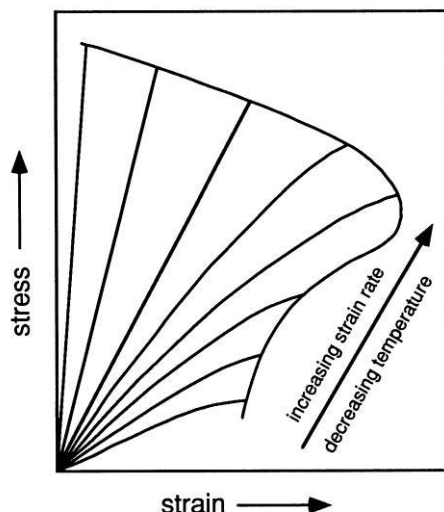


Figure 4-22 Effect of temperature and strain rate on the stress-strain curve.

Creep tests can be made in shear, torsion, flexure, or compression modes, as well as in tension. Results of these tests are particularly important for selecting a polymer that must sustain loads for long periods. Usually, the parameter of interest is the tensile *compliance*, D , which is the ratio of strain to stress. While the stress, σ_0 , is held constant during a creep test, the strain depends upon the time during which the load has been applied and, therefore, the compliance also becomes a function of time as

$$D(t) = \frac{\varepsilon(t)}{\sigma_0}. \quad (4.60)$$

The response of different materials—ideal elastic, ideal viscous, and viscoelastic—to a step change in stress (or load) is illustrated in Figure 4-23. For an ideal (Hookean) elastic material, the resulting strain is instantaneous and constant during the duration of the applied stress. When the load is removed at $t = t'$, the strain instantaneously drops to zero (Figure 4-23A). This follows from Hooke's law applied to the case of a constant stress:

$$\varepsilon = D\sigma_0 = \varepsilon_0. \quad (4.61)$$

In the case of an ideal (Newtonian) viscous fluid, the strain response is obtained by integration of Newton's law of viscosity ($\sigma = \eta \dot{\varepsilon}$) arranged as

$$\varepsilon = \int_0^t (\sigma_0 / \eta) dt = (\sigma_0 / \eta) t. \quad (4.62)$$

Here, the strain increases linearly with increasing time until the load is removed at $t = t'$, at which time the strain remains constant ($\sigma_0 t' / \eta$) in time (Figure 4-23B) unless an additional load is applied. The deformation is said to be permanent since no elastic recovery is possible.

In the case of a viscoelastic material, recovery can occur due to the elastic contribution of the material. For viscoelastic materials, the strain response will have some of the character of both elastic and viscous materials, as shown in Figure 4-23C. The initial portion of the strain recovery is elastic (i.e., instantaneous) while full recovery is delayed to longer times due to the viscous contribution. The actual viscoelastic response can be reasonably modeled by analyzing the strain response of series or parallel combinations of ideal elastic springs and ideal viscous dashpots (shock absorbers) as discussed in Section 5.1.2.

Instrumentation for creep testing can be a simple laboratory setup whereby a plastic film or bar is clamped at one end to a rigid support (normally enclosed in a temperature-controlled chamber) and a weight is added to the opposite end. The deformation of the loaded specimen is then measured by following the relative movement of two marks, inscribed on the sample, by means of a cathetometer, or traveling microscope.

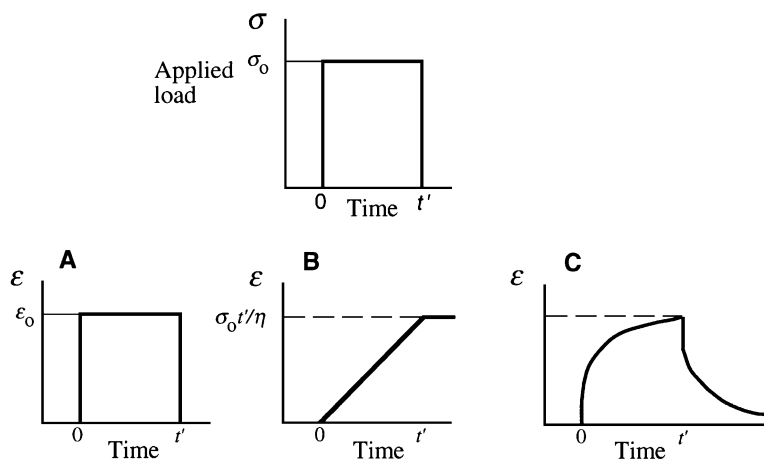


Figure 4-23 Response of different idealized materials to an instantaneous application of a stress at $t = 0$. **A.** Elastic. **B.** Viscous. **C.** Viscoelastic.

Typical creep curves of a low- T_g polymer measured over four decades of time and at several temperatures are shown in Figure 4-24A. As illustrated, creep compliance increases with increasing temperature. This means that the sample softens as temperature is increased, as experience would suggest. As discussed later in Chapter 5 (Section 5.1.6), individual creep curves obtained at different temperatures over short time periods (Figure 4-24A) can be shifted horizontally to yield a master curve at a given temperature and cover a wider range of temperatures. Such a creep master curve showing three regions of viscoelastic behavior is illustrated in Figure 4-24B.

Stress-relaxation experiments can be conveniently performed with the same commercial instruments used in tensile tests. Since deformation must be as close as possible to being instantaneous, the preferred instrumentation is hydraulically driven, rather than screw-driven, tensile testing machines. A rapid extension is applied to the sample and the stress on the sample is measured as a function of time by means of a force transducer. In a stress-relaxation experiment, stress is a function of time and, therefore, the stress-relaxation modulus, E_r ,

$$E_r(t) = \frac{\sigma(t)}{\epsilon_0} \quad (4.63)$$

is also time dependent. Typical stress-relaxation curves are shown in Figure 4-25.

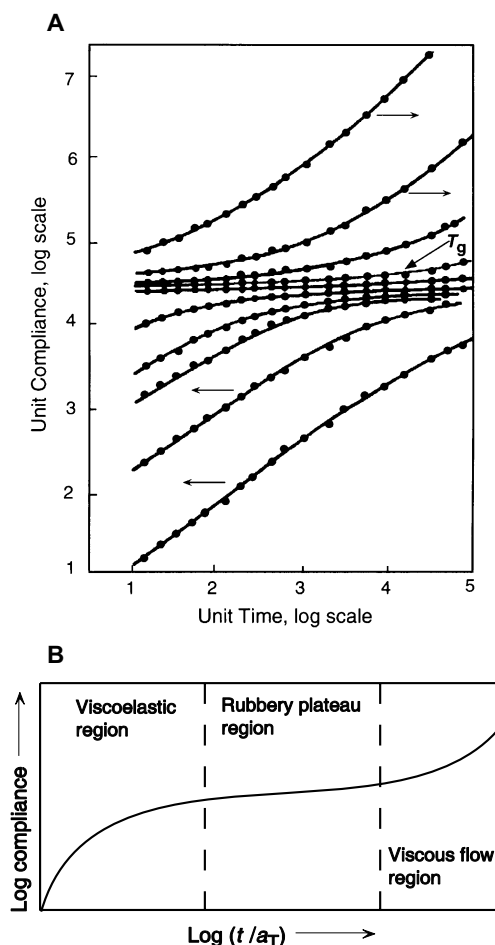


Figure 4-24 **A.** Plots of creep compliance as a function of time at different temperatures. Arrows show direction of the horizontal shift of data to obtain a master curve at a reference temperature taken as the T_g of the polymer. **B.** Creep master curve obtained by time-temperature superposition.

The measurement of a full range of stress-relaxation (or creep-compliance) behavior at a given temperature can take years. Fortunately, it is possible to shift data taken over shorter time periods but at different temperatures to construct a master curve covering a longer time scale at some reference temperature. The principle that allows horizontal shifting of data is called *time-temperature superposition*, which is discussed in Section 5.1.6. The result of this shifting of data over a limited time span to form a master curve was shown for creep compliance in Figure 4-24 and is shown for stress-relaxation modulus in Figure 4-25.

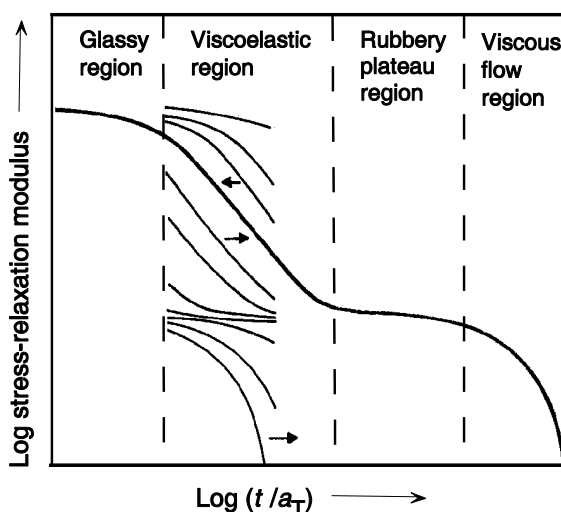


Figure 4-25 Stress-relaxation modulus as a function of time. Arrows show directions of shift to obtain a master curve at reference temperature.

Impact Testing. Impact tests measure the energy expended up to failure under conditions of rapid loading. There are a number of different types of impact tests. These include the widely used Izod and Charpy tests in which a hammer-like weight strikes a specimen and the energy-to-break is determined from the loss in the kinetic energy of the hammer. Other variations include the falling ball or dart test, whereby the energy-to-break is determined from the weight of the ball and the height from which it is dropped. Values of impact strength may also be calculated from the area under the stress-strain curve in high-speed tensile tests. Instrumented impact testing provides a complete report of the load applied to the specimen during the entire impact event and yields information on deformation and fracture processes [30].

Information obtained from impact tests may be used to determine whether a given plastic has sufficient energy-absorbing properties to be useful for a particular application, such as plastics for beverage bottles or window replacement. In such cases, it is important that the material be tested at temperatures and impact conditions close to those of actual use because impact strength will decrease with decreasing temperature and with increasing rate of deformation. The presence of defects that act as stress concentrators will also reduce impact strength. In order to standardize impact results or to study the effect of cracks and other defects on impact properties, samples with inscribed notches of specified dimensions are often used. Typical values of notched-Izod impact strengths for several important polymers are given in Table 4-15. Brittle polymers, such as polystyrene, have very low

impact strengths, while many engineering thermoplastics (e.g., polycarbonate) are very impact resistant.

Table 4-15 Values of Notched-Izod Impact Strength for Some Representative Thermoplastics

Polymer	Impact Strength ^a (J m ⁻¹)
Polystyrene	13–21
Poly(vinyl chloride)	21–160
Polypropylene	27–107
Polystyrene (high-impact)	27–427
Polyethylene (high-density)	27–1068
ABS	53–534
Polysulfone	69–267
Polycarbonate	641–961
Polyethylene (low-density)	854

^a To convert J m⁻¹ to ft-lb/in.⁻¹, divide by 53.38.

Generally, amorphous polymers with large bulky substituent groups and nonlinear backbones are brittle. Unoriented crystalline structure also contributes to brittleness in polymers whose T_g is above the testing temperature. Some correlation may exist between the presence of pronounced low-temperature secondary relaxations corresponding to small-scale motions of the chain backbone and the impact properties of many ductile polymers. Brittle polymers can be made to be more impact resistant by dispersing small ($<0.1\text{-}\mu\text{m}$ -diameter) rubber particles within the polymer matrix, as in the case of high-impact polystyrene (HIPS) and ABS resins (see Section 7.2.2). Good adhesion between the rubbery inclusions and brittle matrix polymers is important for high impact resistance and is typically achieved by grafting the rubber and matrix (glassy) polymers.

Fatigue Testing. Fatigue tests are used to determine the number of cycles (N) of applied strain at a given level of stress that a sample can sustain before complete failure. This number of cycles to failure is called the *fatigue life*. The *endurance limit* is the maximum value of applied stress for which failure will not occur regardless of how many cycles the stress is applied. Typically, the value of stress leading to failure at a given N is 20% to 40% of the static tensile strength. The fatigue life decreases with increasing frequency of oscillation and as temperature is decreased. Information obtained by means of fatigue tests is extremely important in evaluating engineering and composite materials considered for load-bearing applications or when frequent periodic stress loading may be encountered, as for example in a plastic hinge joint. A representative fatigue curve is illustrated in Figure 4-26.

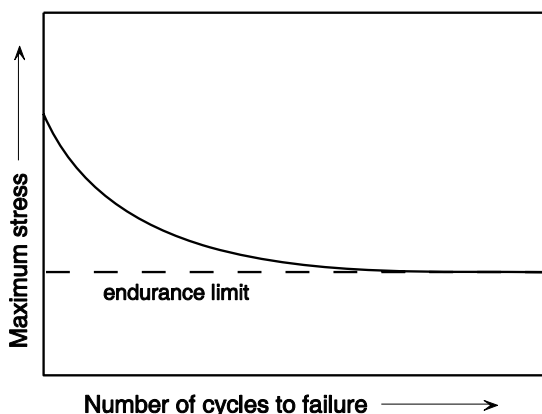


Figure 4-26 Representative fatigue curve.

4.5 Solid-State Characterization Methods

4.5.1 Microscopy

All types of microscopy, including optical and electron microscopy, have been used to investigate the morphology of polymeric materials. These include crystalline polymers, block copolymers, polymer blends, fibers, and composites. In this chapter, Figure 4-5 showed crystalline spherulites of polypropylene as seen by scanning electron microscopy (SEM). A scanning electron micrograph of the craze structures of poly(2,6-dimethyl phenylene oxide) was shown in Figure 4-16. Other illustrations appear in several chapters in this text.

Polymer surface morphology can be characterized at high magnification and resolution by traditional methods of electron microscopy such as SEM and transmission electron microscopy (TEM). During the 1980s, two related methods—scanning tunneling microscopy (STM) and atomic force microscopy (AFM) [31]—were introduced. This new class of microscopy, especially AFM, offered superior resolution with few of the specialized sample preparations such as microtomy, etching, staining, or gold coating that are required for SEM and TEM studies. AFM can be used to investigate polymer crystallinity [32, 33] and for characterizing the surface morphology of polymer films, fibers, coatings, and injection-molded parts at high magnification and resolution up to 0.1 nm. ATM is used particularly for characterizing multiphase polymer systems. As illustrated in Figure 4-27A, both AFM and STM employ a very sharp tip to probe and map the morphology of the surface; however, both the tip and polymer surface need to be conductive for STM measurements, which limits its applicability to polymers. The tip in AFM is typically

silicon (or silicon nitride) with a ~10–20-nm apex diameter mounted on a rectangular silicon cantilever. Tip–surface interactions can occur by van der Waals, electrical, or magnetic forces [34] that are measured by deflection of the cantilever. An atomic force micrograph showing the detailed lamellae structure of a propylene–ethylene copolymer is shown in Figure 4-27B.

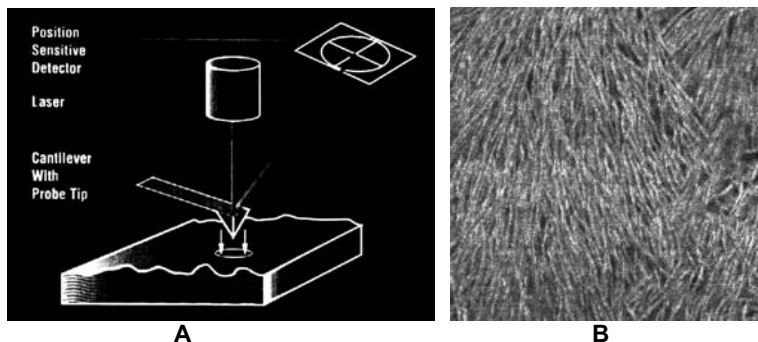


Figure 4-27 **A.** Basic design of an atomic force microscope [33]. Annual Review of Materials Science by Annual Reviews. Reproduced with permission of Annual Reviews in the format. Reproduced in a book via Copyright Clearance Center. **B.** AFM phase image showing radial orientation of crystalline lamellae in a film of a propylene–ethylene random copolymer (15 mole % ethylene) crystallized at 45°C. Courtesy of R. Alamo.

4.5.2 Scattering Methods

A variety of scattering methods have been used for polymer characterization. Light scattering of dilute polymer solutions to determine weight-average molecular weight and chain conformations was discussed in Section 3.3.2. As covered in Section 4.2.4, wide-angle X-ray scattering (WAXS) can be used to determine the fractional crystallinity of semicrystalline polymers and to determine the Bragg spacing [16]. Polymers also can be characterized by small-angle neutron, X-ray, and light scattering [35]. In the case of light scattering, scattering contrast depends upon the difference between the refractive indices of the polymer and its surroundings. Light scattering is useful when the characteristic dimension (D) of the scatterer is greater than $\lambda/4\pi$ where λ is the wavelength of light. Neutron scattering can provide information about both the structure and dynamics of a polymer system. Thermal neutrons have wavelengths in the 2–25 Å range. Examples where small-angle neutron scattering (SANS) has been used to study structure include polymer solutions, blends, gels, nanomaterials, membranes, micelles, and grafted and branched polymers [36].

SUGGESTED READING

ENTANGLEMENTS

- de Gennes, P.-G., *Entangled Polymer*. Physics Today, June 1983, p. 33.
- Porter, R. S., and J. F. Johnson, *The Entanglement Concept in Polymer Systems*. Chemical Reviews, 1966. **66**: p. 1.
- Porter, R. S., W. J. MacKnight, and J. F. Johnson, *Viscous and Elastic Behavior Attributed to Polymer Entanglements*. Rubber Chemistry and Technology, 1967. **40**: p. 1.

THE GLASSY STATE

- Eisenberg, A., *The Glassy State and the Glass Transition*, in *Physical Properties of Polymers*. 2nd ed. J. E. Mark, A. Eisenberg, W. W. Graessley, L. Mandelkern, E. T. Samulski, J. L. Koenig, and G. D. Wignall, eds. 1993, Washington, DC: American Chemical Society, p. 61.
- Goldstein, M. and R. Simha, eds., *The Glass Transition and the Nature of the Glassy State*. Annals of the New York Academy of Sciences, 1976. **279**: p. 68.
- Haward, R. N., ed., *The Physics of Glassy Polymers*. 1973, New York: John Wiley & Sons.
- Hutchinson, J., *Physical Aging of Polymers*. Progress in Polymer Science, 1995. **20**: p. 703.

CRYSTALLINITY

- Long, Y., R. A. Shanks, and Z. H. Stachurski, *Kinetics of Polymer Crystallisation*. Progress in Polymer Science, 1995. **20**: p. 651.
- Mandelkern, L., *The Crystallization of Flexible Polymer Molecules*. Chemical Reviews, 1956. **56**: p. 903.
- Mandelkern, L., *The Crystalline State*, in *Physical Properties of Polymers*. 2nd ed. J. E. Mark, A. Eisenberg, W. W. Graessley, L. Mandelkern, E. T. Samulski, J. L. Koenig, and G. D. Wignall, eds. 1993, Washington, DC: American Chemical Society, 1993, p. 145–200.
- Philips, P. J., *Polymer Crystals*. Reports on Progress in Physics, 1990. **53**: p. 549.
- Samuels, R. J., *Structured Polymer Properties*. 1974, New York: John Wiley & Sons.
- Sanchez, I. C., *Modern Theories of Polymer Crystallization*. Journal of Macromolecular Science—Reviews in Macromolecular Chemistry, 1974. **C10**: p. 113.
- Sanchez, I. C., and E. A. DiMarzio, *Dilute Solution Theory of Polymer Crystal Growth: A Kinetic Theory of Chain Folding*. Journal of Chemical Physics, 1971. **55**: p. 893.
- Sanchez, I. C., and R. K. Eby, *Crystallization of Random Copolymers*. Journal of Research National Bureau of Standards, 1973. **77A**: p. 353.
- Schultz, J. M., *Polymer Crystallization*. 2001, Washington DC: American Chemical Society.

MECHANICAL PROPERTIES

- Aklonis, J. J., *Mechanical Properties of Polymers*. Journal of Chemical Education, 1981. **58**: p. 892.
- Boyd, R. H., *The Conformational Analysis of Crankshaft Motions in Polyethylene*. Macromolecules, 1974. **7**: p. 855.

- Hutchinson, J. H., *Physical Aging of Polymers*. Progress in Polymer Science, 1995. **20**: p. 703.
- Nielsen, L. E., *Cross-Linking Effect on Physical Properties of Polymers*. Journal of Macromolecular Science—Review in Macromolecular Chemistry, 1969. **C3**: p. 69.
- Savadori, A., *Impact Testing of Plastics: Present Knowledge*. Polymer Testing, 1985. **5**: p. 209.
- Stachurski, Z. H., *Deformation Mechanisms and Yield Strength in Amorphous Polymers*. Progress in Polymer Science, 1997. **22**: p. 407.
- Ward, I. M., and D. W. Hadley, *An Introduction to the Mechanical Properties of Solid Polymers*. Chichester: John Wiley & Sons, 1993.

CHARACTERIZATION METHODS

- Bershtein, V. A., and V. M. Egorov, *Differential Scanning Calorimetry of Polymers*. Chichester: Ellis Horwood, 1994.
- Roe, R.-J., *Methods of X-Ray and Neutron Scattering in Polymer Science*. New York: Oxford University Press, 2000.
- Sawyer, L. C., and D. T. Grubb, *Polymer Microscopy*. 1987, London: Chapman and Hall.
- Stein, R. S., and M. Srinivasarao, *Fifty Years of Light Scattering: A Perspective*. Journal of Polymer Science: Part B: Polymer Physics, 1993. **31**: p. 2003.
- Turi, E. A., ed., *Thermal Characterization of Polymeric Materials*. 1981, New York: Academic Press.
- Wunderlich, B., *Thermal Analysis of Macromolecules*. Journal of Thermal Analysis, 1996. **46**: p. 643.
- Zoller, P., and D. Walsh, *Standard Pressure–Volume–Temperature Data for Polymers*. 1995, Lancaster, PA: Technomic.

PROBLEMS

- 4.1** Show that $\sigma^T = \sigma(1 + \varepsilon)$ for an incompressible material.
- 4.2** A tensile strip of polystyrene that is 10 cm in length, 5 cm in width, and 2 cm in thickness is stretched to a length of 10.5 cm. Assuming that the sample is isotropic and deforms uniformly, calculate the resulting width and the percent volume change after deformation.
- 4.3** A polymer has a crystalline growth parameter (n) of 2 and a rate constant (k) of 10^{-2} s^{-2} at 100°C . The polymer is melted and then quenched to 100°C and allowed to crystallize isothermally. After 10 s, what is the percent crystallinity of the sample?
- 4.4** What is the percent volume change that is expected at 100% elongation of natural rubber, assuming that no crystallization occurs during deformation?
- 4.5** Give your best estimate for the weight fraction of plasticizer required to lower the T_g of poly(vinyl chloride) (PVC) to 30°C . Assume that the T_g of PVC is 356 K and that of the plasticizer is 188 K. No other information is available.

4.6 Show that the inverse rule of mixtures given by eq. (4.35) can be obtained from the generalized relationship given by eq. (4.33) when $T_{g,1} \approx T_{g,2}$.

4.7 Polytetrafluoroethylene has been reported to exhibit a negative Poisson ratio. Explain why this polymer exhibits this unusual behavior.

4.8 A sample of poly(ethylene terephthalate) is reported to be 20% crystalline.

(a) What is the expected density of this sample?

(b) What is the expected specific heat increment of this semicrystalline sample?

(c) What is the expected heat of fusion of this sample?

4.9 Twenty wt% of a styrene oligomer having a number-average degree of polymerization of 7 is mixed with a commercial polystyrene sample having a number-average molecular weight of 100,000.

(a) What is the T_g (K) of the styrene oligomer?

(b) What is the T_g (K) of the polystyrene mixture?

4.10 The 1% secant modulus of a polystyrene sample is 3 GPa.

(a) What is the nominal stress (MPa) of this sample at a nominal strain of 0.01?

(b) What is the true stress (MPa) of this sample at a nominal strain of 0.01?

(c) What is the percent change in volume of this sample at the nominal strain of 0.01?

4.11 If the Young's modulus of a sample of polystyrene is determined to be 3 GPa at room temperature, calculate its shear modulus.

4.12 Isotactic poly(methyl methacrylate) has a much lower T_g than the corresponding syndiotactic polymer. How can isotactic and syndioactic PMMA be polymerized? Explain why the isotactic polymer has the lower T_g .

REFERENCES

1. Wool, R. P., *Polymer Entanglements*. Macromolecules, 1993. **26**: p. 1564–1569.
2. Graessley, W. W., *The Entanglement Concept in Polymer Rheology*. Advances in Polymer Science, 1974. **16**: p. 1–179.
3. Heymans, N., *Diffuse versus Point Entanglements—Homopolymers and Blends*. Journal of Materials Science, 1986. **21**: p. 1919–1926.
4. de Gennes, P. G., *Reptation of a Polymer Chain in the Presence of Fixed Obstacles*. Journal of Chemical Physics, 1971. **55**(2): p. 572–579.
5. Klein, J., *Evidence for Reptation in an Entangled Melt*. Nature, 1978. **271**(5641): p. 143–145.

6. Cohen, M. H., and D. Turnbull, *Molecular Transport in Liquids and Glasses*. Journal of Chemical Physics, 1959. **31**(5): p. 1164–1169.
7. van Krevelen, D. W., *Properties of Polymers*. 3rd ed. 1990, Amsterdam: Elsevier.
8. Gibbs, J. H., and E. A. DiMarzio, *Nature of the Glass Transition and the Glassy State*. Journal of Chemical Physics, 1958. **28**(3): p. 373–383.
9. Boyd, R. H., and S. M. Breitling, *The Conformational Analysis of Crankshaft Motions in Polyethylene*. Macromolecules, 1974. **7**(6): p. 855–862.
10. Fried, J. R., *Sub- T_g Transitions*, in *Physical Properties of Polymers Handbook*, J. E. Mark, ed. 2007, New York: Springer, p. 217–232.
11. Tanaka, T., Y. Chatani, and H. Tadokoro, *Crystal Structure of Polyisobutylene*. Journal of Polymer Science: Polymer Physics Edition, 1974. **12**: p. 515–531.
12. Stein, R. S., *A Comment on “Incompatible Blends: Thermal Effects in a Model System”*. Journal of Polymer Science: Polymer Physics Edition, 1981. **19**: p. 1281.
13. Avrami, M., *Kinetics of Phase Change. I. General Theory*. Journal of Chemical Physics, 1939. **7**: p. 1103–1112.
14. Avrami, M., *Kinetics of Phase Change. II. Transformation-Time Relations for Random Distribution of Nuclei*. Journal of Chemical Physics, 1940. **8**: p. 212–224.
15. Phillips, P. J., and H. T. Tseng, *Influence of Pressure on Crystallization in Poly(ethylene terephthalate)*. Macromolecules, 1989. **22**: p. 1649–1655.
16. Mo, Z., and H. Zhang, *The Degree of Crystallinity in Polymers by Wide-Angle X-Ray Diffraction (WAXD)*. Journal of Macromolecular Science—Reviews in Macromolecular Chemistry and Physics, 1995. **35**: p. 555–580.
17. Ehrenfest, P., Leiden Comm. Suppl., 1933. **76b**.
18. Flory, P. J., L. Mandelkern, and H. K. Hall, *Crystallization in High Polymers. VII. Heat of Fusion of Poly(*N,N*-sebacoylpiperazine) and Its Interaction with Diluents*. Journal of the American Chemical Society, 1951. **73**: p. 2532–2538.
19. Simha, R., and R. F. Boyer *On a General Relation Involving the Glass Temperature and Coefficients of Expansion of Polymers*. Journal of Chemical Physics, 1962. **37**(5): p. 1003–1007.
20. Fox, T. G., and P. J. Flory, *Second-Order Transition Temperatures and Related Properties of Polystyrene. I. Influence of Molecular Weight*. Journal of Applied Physics, 1950. **21**: p. 581–591.
21. Boyer, R. F., *Variation of Polymer Glass Transition Temperatures with Molecular Weight*. Macromolecules, 1974. **7**(1): p. 142–143.
22. Kelley, F. N., and F. Bueche, *Viscosity and Glass Temperature Relations for Polymer-Diluent Systems*. Journal of Polymer Science, 1961. **50**: p. 549–556.
23. Couchman, P. R., and F. E. Karasz, *A Classical Thermodynamic Discussion of the Effect of Composition on Glass-Transition Temperatures*. Macromolecules, 1978. **11**(1): p. 117–119.
24. Fried, J. R., and S.-Y. Lai, *Experimental Assessment of the Thermodynamic Theory of the Composition Variation of T_g : PVC Systems*. Journal of Applied Polymer Science, 1982. **27**: p. 2869–2883.
25. Judovits, L. H., et al., *The Heat Capacity of Solid and Liquid Polystyrene, *p*-Substituted Polystyrenes, and Crosslinked Polystyrenes*. Journal of Polymer Science: Part B: Polymer Physics, 1986. **24**: p. 2725–2741.
26. Moynihan, C. T., et al., *Dependence of the Glass Transition Temperature on Heating and Cooling Rate*. Journal of Physical Chemistry, 1974. **78**: p. 2673–2677.
27. Fox, T. G., and S. Loshaek, *Influence of Molecular Weight and Degree of Crosslinking on the Specific Volume and Glass Temperature of Polymers*. Journal of Polymer Science, 1955. **15**: p. 371–390.

28. Kambour, R. P., and A. S. Holik, *Electron Microscopy of Crazes in Glassy Polymers: Use of Reinforcing Impregnants during Microtomy*. Journal of Polymer Science: Part A-2, 1969. **7**: p. 1393–1403.
29. Seitz, J. T., *The Estimation of Mechanical Properties of Polymers from Molecular Structure*. Journal of Applied Polymer Science, 1993. 1331-1351.
30. Radon, J. C., *Application of Instrumented Impact Test in Polymer Testing*. Journal of Applied Polymer Science, 1978. **22**: p. 1569-1581.
31. Binnig, G., C. F. Quate, and C. Gerber, *Atomic Force Microscope*. Physical Review Letters, 1986. **56**(9): p. 930-933.
32. Hobbs, J. K., O. E. Farrance, and L. Kailas, *How Atomic Force Microscopy Has Contributed to Our Understanding of Polymer Crystallization*. Polymer, 2009. **50**: p. 4281-4292.
33. Magonov, S. N., and D. H. Reneker, *Characterization of Polymer Surfaces with Atomic Force Microscopy*. Annual Review of Materials Science, 1997. **27**: p. 175-222.
34. Meyer, E., *Atomic Force Microscopy*. Progress in Surface Science, 1992. **41**: p. 3-49.
35. Higgins, J. S., and R. S. Stein, *Recent Developments in Polymer Applications of Small-Angle Neutron, X-ray and Light Scattering*. Journal of Applied Crystallography, 1978. **11**: p. 346-375.
36. Hammouda, B., *SANS from Polymers—Review of the Recent Literature*. Journal of Macromolecular Science—Polymer Reviews, 2010. **C50**: p. 14–29.